NASA/TM—2012-217410 AIAA–2012–0069

Flow-Field Surveys For Rectangular Nozzles

K.B.M.Q. Zaman
Glenn Research Center, Cleveland, Ohio

April 2012

NASA STI Program . . . in Profile

Since its founding, NASA has been dedicated to the advancement of aeronautics and space science. The NASA Scientific and Technical Information (STI) program plays a key part in helping NASA maintain this important role.

The NASA STI Program operates under the auspices of the Agency Chief Information Officer. It collects, organizes, provides for archiving, and disseminates NASA's STI. The NASA STI program provides access to the NASA Aeronautics and Space Database and its public interface, the NASA Technical Reports Server, thus providing one of the largest collections of aeronautical and space science STI in the world. Results are published in both non-NASA channels and by NASA in the NASA STI Report Series, which includes the following report types:

- TECHNICAL PUBLICATION. Reports of completed research or a major significant phase of research that present the results of NASA programs and include extensive data or theoretical analysis. Includes compilations of significant scientific and technical data and information deemed to be of continuing reference value. NASA counterpart of peer-reviewed formal professional papers but has less stringent limitations on manuscript length and extent of graphic presentations.

- TECHNICAL MEMORANDUM. Scientific and technical findings that are preliminary or of specialized interest, e.g., quick release reports, working papers, and bibliographies that contain minimal annotation. Does not contain extensive analysis.

- CONTRACTOR REPORT. Scientific and technical findings by NASA-sponsored contractors and grantees.

- CONFERENCE PUBLICATION. Collected papers from scientific and technical conferences, symposia, seminars, or other meetings sponsored or cosponsored by NASA.

- SPECIAL PUBLICATION. Scientific, technical, or historical information from NASA programs, projects, and missions, often concerned with subjects having substantial public interest.

- TECHNICAL TRANSLATION. English-language translations of foreign scientific and technical material pertinent to NASA's mission.

Specialized services also include creating custom thesauri, building customized databases, organizing and publishing research results.

For more information about the NASA STI program, see the following:

- Access the NASA STI program home page at *http://www.sti.nasa.gov*

- E-mail your question via the Internet to *help@sti.nasa.gov*

- Fax your question to the NASA STI Help Desk at 443–757–5803

- Telephone the NASA STI Help Desk at 443–757–5802

- Write to:
  NASA Center for AeroSpace Information (CASI)
  7115 Standard Drive
  Hanover, MD 21076–1320

NASA/TM—2012-217410 AIAA–2012–0069

Flow-Field Surveys For Rectangular Nozzles

K.B.M.Q. Zaman
Glenn Research Center, Cleveland, Ohio

Prepared for the
50th Aerospace Science Conference
sponsored by the American Institute of Aeronautics and Astronautics
Nashville, Tennessee, January 9–12, 2012

National Aeronautics and
Space Administration

Glenn Research Center
Cleveland, Ohio 44135

April 2012

Acknowledgments

Support from the Supersonics Project of the Fundamental Aeronautics Program is gratefully acknowledged. The author would like to thank James Bridges, Franco Frate, Stewart Leib, and Abbas Khavaran for various inputs during this study.

This work was sponsored by the Fundamental Aeronautics Program
at the NASA Glenn Research Center.

Level of Review: This material has been technically reviewed by technical management.

Available from

NASA Center for Aerospace Information
7115 Standard Drive
Hanover, MD 21076–1320

National Technical Information Service
5301 Shawnee Road
Alexandria, VA 22312

Available electronically at http://www.sti.nasa.gov

Flow-Field Surveys For Rectangular Nozzles

K.B.M.Q. Zaman
National Aeronautics and Space Administration
Glenn Research Center
Cleveland, Ohio 44135

Abstract

Flow field survey results for three rectangular nozzles are presented for a low subsonic condition obtained primarily by hot-wire anemometry. The three nozzles have aspect ratios of 2:1, 4:1 and 8:1. A fourth case included has 2:1 aspect ratio with chevrons added to the long edges. Data on mean velocity, turbulent normal and shear stresses as well as streamwise vorticity are presented covering a streamwise distance up to sixteen equivalent diameters from the nozzle exit. These detailed flow properties, including initial boundary layer characteristics, are usually difficult to measure in high speed flows and the primary objective of the study is to aid ongoing and future computational and noise modeling efforts.

Introduction

This report documents flow-field survey results for three rectangular nozzles of aspect ratios 2:1, 4:1 and 8:1 as well as for a fourth 2:1 aspect ratio case with chevrons added to the long edges. The motivation for investigating the rectangular nozzles comes from potential noise benefits, as outlined in Reference 1, (see also Refs. 2 and 3). Several rectangular nozzles with and without chevrons and other potential noise reduction features have been designed and fabricated for flow-field and noise tests. The design considerations and details of these nozzles have been discussed in Reference 4. Four of the nozzles were adopted for the present flow-field surveys at low-speeds. The primary motivation was to provide detailed flow-field and initial boundary layer properties, usually difficult to measure at higher speeds, in order to aid computational fluid dynamics (CFD) investigations leading to noise modeling efforts.

All four nozzles have the equivalent diameter (D) of 2.12 in. Data are also taken with a 2 in. diameter convergent round nozzle for comparison. The surveys are conducted primarily by hot-wire anemometry at a low jet Mach number of 0.226. Centerline velocity profiles at higher jet Mach numbers are also obtained using a Pitot-static probe. Highlights of the results were summarized in a conference paper (Ref. 5). In this technical memorandum, the overall summary for the distribution of various flow properties, comparing the four rectangular nozzle cases, is discussed first. This is followed by a documentation of detailed contours of the properties on cross-sectional planes at various downstream locations. The data files can be found on a supplemental CD (not published on the Web) which may be requested from the NASA Center for AeroSpace Information (CASI) at http://www.sti.nasa.gov, or 443–757–5802. The raw data sets are given in a folder on the supplemental CD entitled "Rectangular_noz_data_files_April_2011". Also included are the coordinates for the four nozzles in a separate folder on the CD; questions or clarification may be directed to any of the authors of Reference 4 (Mr. Franco C. Frate and Dr. James E. Bridges of the NASA Glenn Research Center). All data files are further described in the Appendix at the end of this report.

Experimental Procedure

The experiments were conducted in an open jet facility housed in the Test Cell CW17 of NASA Glenn Research Center; an interested reader may find further description of the facility in Reference 6. As already stated, the four nozzles included an aspect ratio 2:1 (referred to as 'NA2Z' in the earlier design and test plan documents, and referred herein simply as 'R2'), a 2:1 case with chevrons ('NA2C3', referred as 'R2C'), a 4:1 case ('NA4Z', referred as 'R4') and a 8:1 case ('NA8Z', referred as 'R8'). A

picture of the flow facility fitted with the R4 nozzle is shown in Figure 1(a) while the four nozzles are shown in Figure 1(b). The coordinate origin is at the nozzle exit center with y and z denoting lateral coordinates in the horizontal and vertical directions, respectively. A single (TSI 1260A-10) hot-wire, aligned with the nozzle wall, was used for boundary layer surveys approximately 0.04 in. downstream of the nozzle lip. For surveys on cross-sectional (y-z) planes, two (TSI 1241-20) X-wires, one in the '*u-v'* and the other in *'u-w'* configuration, were used to obtain all three components of velocity and turbulent stresses. The turbulent shear stresses $\overline{uv}$ and $\overline{uw}$ as well as mean streamwise vorticity ω_x were also obtained in the surveys.

The hot-wire probes were calibrated at the exit of the round nozzle and the X-wire data were reduced using simple 'cosine law'. For calculation of ω_x, gradient correction was applied for V and W data to account for the errors introduced by separation of the sensors in each X-wire. For further details of the measurement procedures, see Reference 6. The ω_x data close to the nozzle exit (x/D=0.05) were read to be very large in amplitude and thought to be erroneous due to inadequate gradient correction and thus are not shown for that station. On the other hand, the ω_x amplitudes for most cases at the farthest downstream station (x/D=16) were too small and within measurement noise level and thus are also not shown. The averaging time for the measurements at each point is varied from 4 to 10 sec depending on the streamwise location, the longest time being allowed for the farthest downstream location.

The Pitot-static probe had a diameter of 0.065 in. The Pitot port was located at the center of the hemispherical tip and four equally-spaced static ports were located 0.375 in. from the tip. In the calculation of velocities, the measured static pressure was assumed to apply at the tip location. The jet velocity (U_j) was determined from the ratio of the plenum tank pressure and the ambient pressure in the test chamber using one-dimensional isentropic equations. Unless indicated otherwise, the velocities are normalized by the jet velocity U_j and the distances are normalized by the equivalent diameter D. All data pertain to cold flows (i.e., with total temperature the same everywhere as in the ambient of the test chamber).

Results

In the following the exit boundary layer data are presented first. This is followed by profiles of properties along the jet centerline obtained by the single hot-wire as well as the Pitot-static probe. Since the X-wire survey results involve many plots for various properties at various x-stations, the overall trends of these data are discussed next. Trends based on line graphs for the streamwise variation of 'field maxima' are compared for the four nozzles. The detailed survey results on cross-sectional planes at various streamwise locations are shown in Figures A1 to A22 in the Appendix. The data folder, "Rectangular_noz_data_files_April_2011", contains all data files structured for easy use by 'Tecplot' and the plotting routines are also included. Time traces of hot-wire velocity are also included for the three baseline rectangular cases (without chevrons) in the 'BL data' sub folder. These data are taken approximately at 95% velocity point in the boundary layer on the middle of the long edges. To conserve space, the velocity data (in ft/s) are multiplied by 100 and saved as integers. Each trace has 400,000 data points taken at the rate of 100 kHz (i.e., for 4 seconds).

In Figure 2, sample boundary layer profiles are compared for the R2 and R2C nozzles. The mean velocity and turbulence intensity data are shown in Figures 2(a) and 2(b), respectively. The 10% jet velocity point ($y_{0.1}$), as measured, is assumed to be the wall location (recall that the measurement location is slightly downstream and thus the measured velocity does not drop to zero near the wall). While there are some differences in the mean velocity profiles, the turbulence intensity profiles vary significantly between the long and short edges. In either figure it can be seen that the addition of the chevrons (on the long edges) has not made a difference in the profiles measured on the short edge. The measurement locations are indicated in the legend; these are in the middle of the short or long edges except for the 'long edge off-center' case where the measurement is done halfway between the center and the end of the long

edge. The boundary layer characteristics are calculated by integration of the mean velocities between the 98% to 10% velocity points. These are listed in Table 1 and discussed in the following.

Figure 3 shows boundary layer momentum thickness for several values of Reynolds number for the R2 nozzle. Only on the low end of the Re_D range does the data roughly resemble a C/sqrt(Re_D) relationship that would indicate a laminar or 'nominally laminar' state; (C = 0.59 is used to approximately fit the data on the low Re_D range.) From the trends of the data, the boundary layer appears to be 'nominally turbulent' on the higher end of the Re_D range since the thickness does not follow the 'laminar prediction'. However, the shape factors (H_{12}), listed in Table 1, are found to be large that are typical of 'Blassius-type' laminar profiles. Thus, a highly disturbed 'nominally laminar' state is inferred for the boundary layer of the R2 nozzle. Note that the C/sqrt(Re_D) law applies to round nozzles and the behavior at different points of the periphery of a rectangular nozzle may vary. On the other hand, from a consideration of the nature of the velocity fluctuation in the boundary layer, the corresponding states for the R4 and R8 nozzles are inferred to be 'nominally turbulent' (see Refs. 5 and 7). It is also noted that the time traces of the velocity signal do not appear to indicate any dominant periodicity; four such time traces are included in the electronic data folder.

In Figure 4, centerline profiles of mean velocity (U) and streamwise turbulence intensity (u') are compared for the four rectangular cases with data for the round nozzle (denoted as 'Rnd' in the legend). During data acquisition at each measurement point, all quantities were normalized by the current value of jet velocity measured simultaneously. The normalized mean velocity at the nozzle exit often deviated slightly from unity due to calibration drifts. All data were subsequently renormalized by the exit mean velocity so that $U/U_j = 1$. One notes a significant 'vena-contracta' effect with the rectangular cases, i.e., a significant increase in the mean velocity downstream of the nozzle exit. This is more so with the chevron nozzle. The turbulence intensity profiles are shown in Figure 4(b). Unfortunately, even 10 sec averaging was not enough to obtain convergent data and some scatter marks the profiles at the downstream locations. Nevertheless, the relative trends are amply clear. For all rectangular nozzles the peak in the streamwise turbulence intensity profile occurs farther upstream relative to the round nozzle case. The shift in the location of the peak is the most for the highest aspect ratio case of 8:1. The peak intensity increases with decreasing aspect ratio. Note also that the chevrons (R2C) have resulted in a lower amplitude of the peak pushing it farther downstream relative to the baseline 2:1 case (R2). (There was some residual electronic noise in the hot-wire circuitry affecting the measurements at low intensities. The turbulence intensity at the nozzle exit center is thought to be less than 0.5%. However, this has not been looked at rigorously.)

Centerline mean velocity profiles measured by the hot-wire and the Pitot-static probe are compared for the round nozzle in Figure 5 in order to gain some confidence in the consistency of the results. The overall agreement is good; the hot-wire data are also found to repeat well relative to earlier measurements (Ref. 8). Centerline mean velocity profiles obtained by the Pitot-static probe are shown in Figure 6 for the round nozzle for several jet Mach numbers M_j. A lengthening of the potential core with increasing M_j is obvious. The 'asymptotic' slopes of the inverse of the velocities are found to be less (about 0.125) relative to values (about 0.15) reported in Reference 9. This is due to the fact that the measurements did not extend far enough downstream in the present study.

In Figure 7 centerline velocity profiles for the four rectangular cases are compared with the round case at two high subsonic jet Mach numbers. For each rectangular case, by plotting the profiles for the two values of M_j together with the corresponding hot-wire profile from Figure 4(a), a similar downstream shift of the velocity profile may be noted with increasing M_j. This is shown in Figure 8 for the R8 case as an example. It is also apparent from Figure 7 that the 'vena-contracta' effect practically disappears at higher M_j except with the chevron case.

The variation of the maxima of some of the flow properties from the cross-sectional surveys (detailed contours appended in the following), as a function of the streamwise distance, is compared to assess the overall trends. Figure 9 shows such data for the mean streamwise vorticity peak. Streamwise vorticity has negative and positive regions and the maxima here represent that of the absolute values. The vorticity magnitude drops off exponentially with streamwise distance (note the logarithmic ordinate scale). Similar

results were noted earlier in Reference 5. The magnitude is significantly higher for the chevron case. The peak value of streamwise turbulence intensity is similarly compared in Figure 10. Comparison of data for the R2 and R2C cases shows that, except for the upstream-most locations, the peak turbulence has been reduced by the chevrons.

For each of the four rectangular nozzles, the maxima of *u'*, *v'* and *w'* intensities are compared in the four segments of Figure 11. The "anisotropy" in the normal stresses, obvious for all four nozzles, persists to the last measurement station. While the *v'* and *w'* amplitudes are nearly equal the *u'* amplitude is larger at all streamwise locations.

Detailed contours of flow properties are documented in the following figures. These are briefly discussed below. As stated at the end of the Introduction, the raw data can be found in a folder on the supplemental CD entitled "Rectangular_noz_data_files_April_2011".

Figures A1 to A5

Contour plots of the survey results for the R8 nozzle are shown for various downstream locations (*x/D*); the location is indicated in the captions. For each station, the mean velocity (*U*) and three components of turbulence intensity are shown on the left column while the mean streamwise vorticity ω_x and the Reynolds shear stresses are shown on the right column (recall that ω_x is not shown for the first and the last station for most of the cases). Note that on the side of each contour plot the value of the maxima in the field is indicated in parentheses in order to provide an idea about the overall levels. In Figure A2 at *x/D* = 1, concentration of streamwise vorticity into two pairs at the end of the major axis may be noted. Farther downstream only one pair dominates the flow-field as evident from the subsequent figures. At the farthest downstream location of *x/D* = 16 (Fig. A5), the jet cross-section based on the mean velocity as well as the turbulence intensity distributions has become almost round.

Figures A6 to A10

Corresponding contour plots for the R4 nozzle are shown. Similar observations as with the R8 case can be made.

Figures A11 to A16

Corresponding data for the R2 nozzle are shown. Here, for a better assessment of the effect of the chevrons an additional data set is provided for *x/D* = 2 (Fig. A13). Also, while all data are taken covering approximately half of the flow domain, here the full domain is covered at *x/D* = 4 (Fig. A14).

Figures A17 to A22

Results for the chevron (R2C) case are shown similarly in these figures, as done with the baseline (R2) case in Figures A11 to A16. Here, the first axial station is just downstream of the tips of the chevrons. At *x/D* = 1, pairs of streamwise vortices originating from each chevron can be seen. By *x/D* = 4, however, these vortices have merged into two pairs at the ends of the major axis, similar to that in the baseline R2 case (Fig. A14). However, the peak magnitudes are considerably higher in the chevron case. An inspection reveals that the overall turbulence intensities are reduced by the chevrons relative to the R2 case. Compare, for example, the data in Figure A21 with Figure A15 for *x/D* = 8; (see also Fig. 4(b)). However, the amplitudes are higher at upstream locations and the distributions are complex (compare Fig. A18 with A12 for *x/D* = 1).

The reduction in the intensities at the downstream locations has taken place with all three components of turbulence. The overall reduction in turbulence suggests a noise reduction by the chevrons.

Concluding Remarks

Flow field properties for rectangular nozzles of three aspect ratios, including one case with chevrons, are documented in this paper. The data trends are compared with corresponding results from a round nozzle. For the rectangular cases, the peak in the streamwise turbulence intensity profile, measured along the centerline, occurs farther upstream relative to the round case. The shift in the location of the peak is the most for the highest aspect ratio case of 8:1 covered in the experiment. With decreasing aspect ratio the peak intensity is seen to increase. The chevrons result in lower amplitude of the peak pushing it farther downstream relative to the corresponding baseline case. From the flow field surveys, it is noted that, except for locations closest to the nozzle, the turbulence intensities are generally reduced by the chevrons. For all cases, the field maxima of the streamwise component of turbulence intensity is found to be significantly larger than the lateral components; the 'anisotropy' persists to the farthest measurement station of $x/D = 16$. It is hoped that these detailed flow field results may be useful in computational and noise prediction efforts and also advance the understanding of the noise mechanisms for the rectangular jets as well as for the effect of the chevrons.

Appendix—Data Files

The following is a description of the data files accompanying this TM. The data files can be found on a supplemental CD (not published on the Web) which may be requested from the NASA Center for AeroSpace Information (CASI) at http://www.sti.nasa.gov, or 443–757–5802.

Nozzle coordinates.—These are data files for nozzle coordinates. The four files starting with 'N' are for the four nozzles. The three files starting with 'D' are for the transition pieces connecting the aspect ratio 2, 4 and 8 nozzles with a common round receptacle. Any CAD program should be able to import these files for viewing the different pieces of hardware. These files can also be assembled and with some effort used for grid generation for the four nozzle cases for numerical simulations.

X-wire surveys.—These are X-wire survey data for the nozzles as annotated in the file name. The measurement stations are at x/D = 0.05, 1, 4, 8 and 16, except for R2C nozzle where the first measurement station is at x/D = 0.38. For R2 and R2C cases, additional data sets at x/D = 2 are provided. For each nozzle case, separate folders contain data for each x-station. While examples of U, $u'$and ω_x data are discussed in the TM, each folder also include data files for v', w', $\overline{uv}$ and $\overline{uw}$ (all nondimensionalized by jet velocity (U_j) and nozzle equivalent diameter (D)). [Notes: (1) Plot routines are included for convenience; (2) In the data files, U is represented by 'ubv', u' by 'ur', v' by 'vr', w' by 'wr' and ω_x by 'wx'; (3) the quadrants of survey are indicated in the file title.]

BL_profiles.—These are single hot-wire data for the exit boundary layer profiles. The measurement locations as well as the jet velocity in ft/s are annotated in the names of some of the data files. (Example: 'y_survey_R2_long_offcntr_anlzd' indicate profile at a location midway between the end and the center of the long edge of the R2 nozzle). Files not having annotation for measurement location represent profiles in the middle of the long edge. [Notes: (1) Plot routines are included for convenience; (2) In the data files, *y1* (first column) represents the radial location relative to the approximate location of the nozzle wall, negative values being towards the axis of the nozzle.]

Also included are four time series data at 95% velocity points in the boundary layer. The velocity data (in ft/s) are multiplied by 100 and recorded as integers. Each trace has 400,000 data points taken at the rate of 100 kHz (i.e., for 4 seconds).

Centerline profiles.—These are centerline profiles measured by hot-wire or Pitot-static probe; the measurement method is annotated in the file names. For the Pitot-static data files, the jet velocity in ft/s is also annotated with the names. In the hot-wire data files, the three columns of data represent normalized axial distance, mean velocity and turbulence intensity. In the Pitot-static data files, the three columns represent normalized axial distance, normalized mean velocity and current jet velocity in ft/s. [Note: Plot routines are included for convenience].

Profiles of max field values.—These are field maxima of various properties as a function of axial distance. The five columns of data represent normalized axial distance, u', v', w' and ω_x. [Note: Plot routines are included for convenience].

TABLE 1.—EXIT BOUNDARY LAYER CHARACTERISTICS

Nozzle	Location	U_j (ft/s)	δ_2 (in.)	H_{12}	u'_{max}
R2	Short edge	256	0.0034	2.14	0.090
R2	Long mid	256	0.0038	2.55	0.130
R2	Long off-center	256	0.0033	2.46	0.139
R2C	Short edge	256	0.0033	2.13	0.090
R4	Short edge	256	0.0040	1.79	0.110
R4	Long mid	256	0.0030	2.23	0.113
R4	Long off-center	256	0.0026	2.33	0.109
R8	Short edge	256	0.0044	1.91	0.110
R8	Long mid	256	0.0032	1.97	0.107
R8	Long off-center	256	0.0028	2.20	0.101
R2	Long mid	56	0.0045	2.16	0.143
R2	Long mid	79	0.0041	2.14	0.144
R2	Long mid	98	0.0038	2.16	0.149
R2	Long mid	146	0.0036	2.21	0.147
R2	Long mid	221	0.0037	2.51	0.139
R2	Long mid	257	0.0040	2.73	0.137
R2	Long mid	276	0.0042	2.77	0.130
R2	Long mid	297	0.0042	2.80	0.130
R2	Long mid	341	0.0043	2.83	0.132

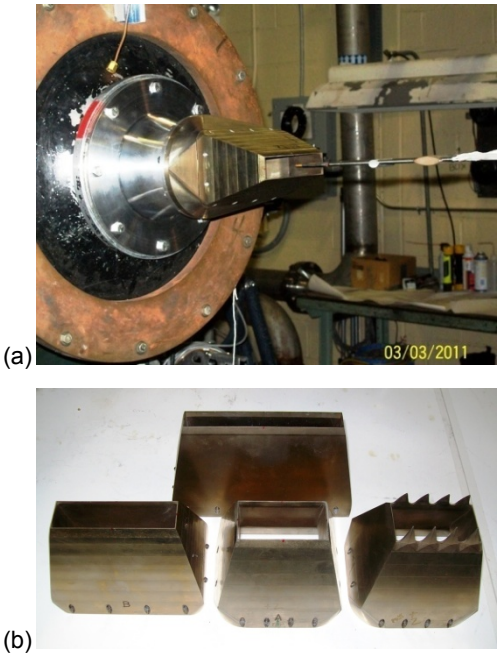

Figure 1.—Experimental facility. (a) Open Jet with 4:1 rectangular (R4) nozzle; the x-wires probes are in foreground. (b) Four nozzles.

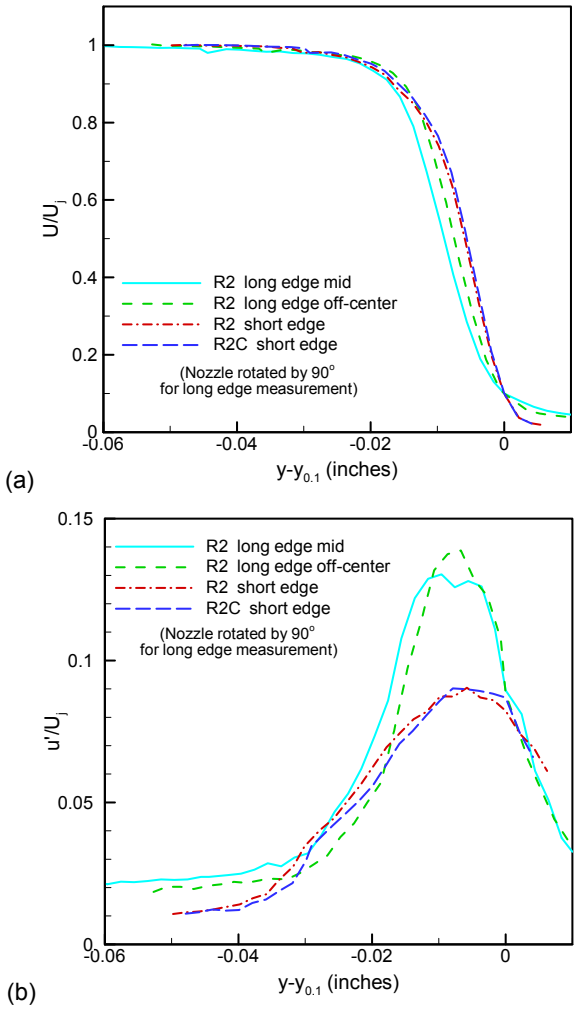

Figure 2.—Exit boundary layer profiles for 2:1 nozzle with and without chevrons at $U_j \approx 256$ ft/s; (a) mean velocity, (b) turbulence intensity.

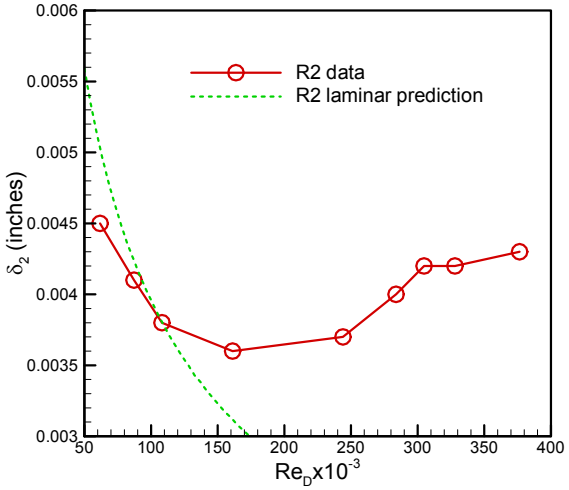

Figure 3.—Exit boundary layer momentum thickness vs. Re_D for R2 nozzle. Measurement at middle of long edge.

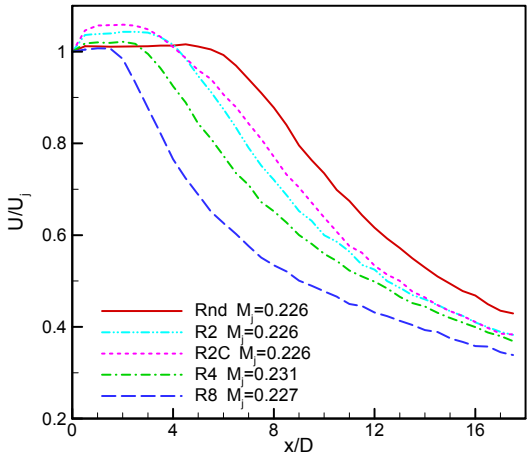

(a)

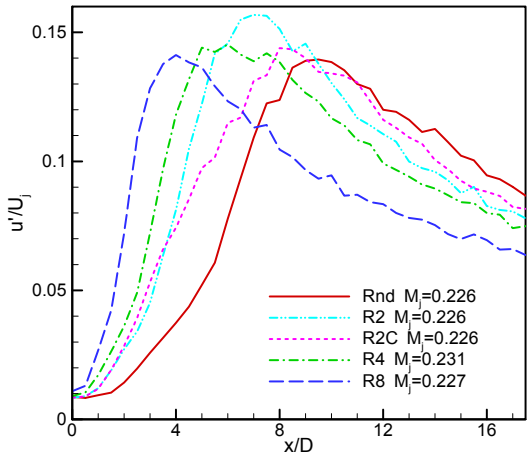

(b)

Figure 4.—Comparison of (a) centerline mean velocity and (b) turbulence intensity profiles. Hot-wire data at $U_j \approx 256$ ft/s.

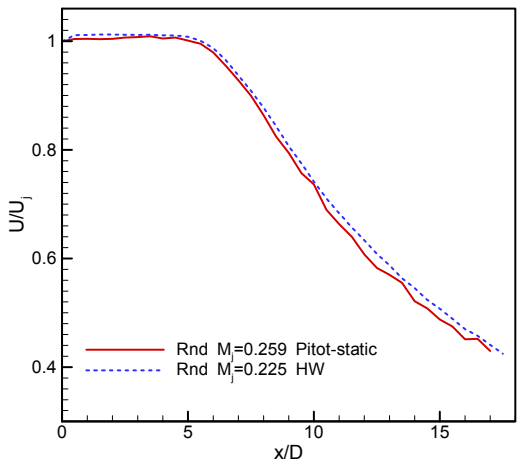

Figure 5.—Centerline mean velocity profiles for Round jet. Comparison of HW and Pitot-static data.

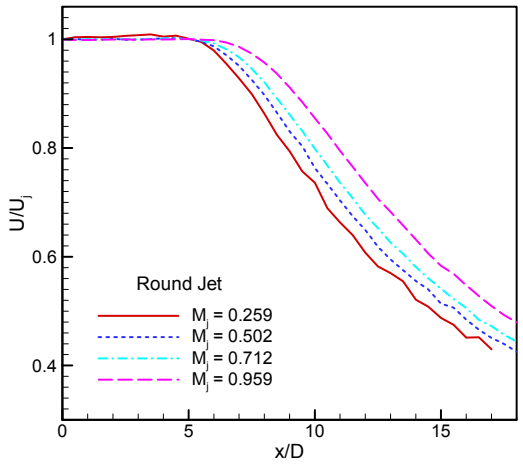

Figure 6.—Centerline mean velocity profiles for Round jet. Pitot-static data showing Mach number effect.

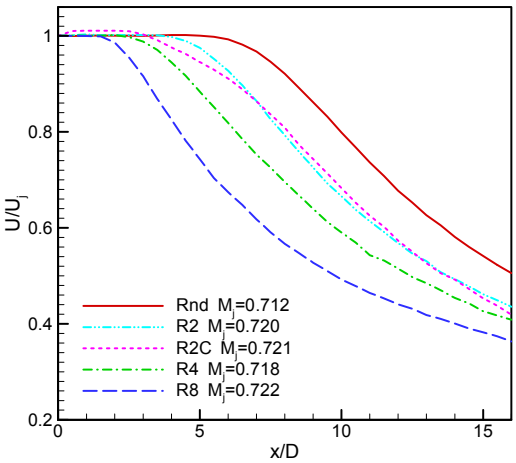

(a)

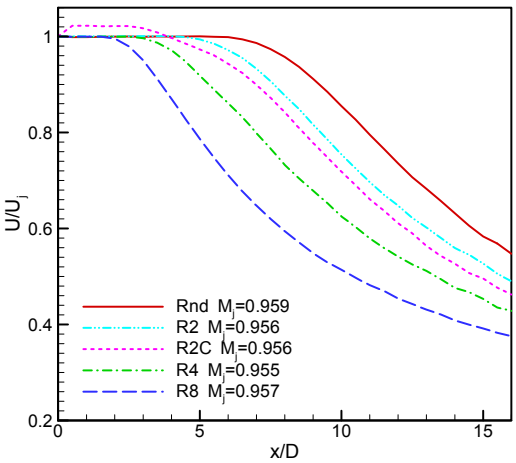

(b)

Figure 7.—Comparison of centerline velocity profiles for different nozzles at (a) $M_j \approx 0.72$ and (b) $M_j \approx 0.96$.

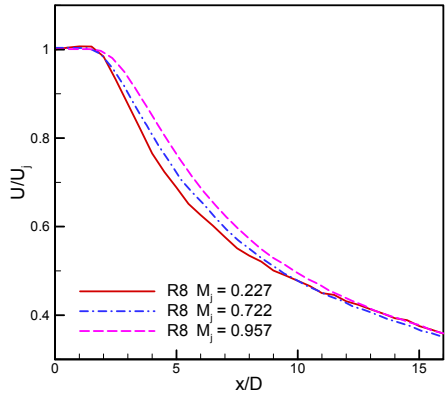

Figure 8.—Centerline mean velocity profiles for R8 case showing Mach number effect.

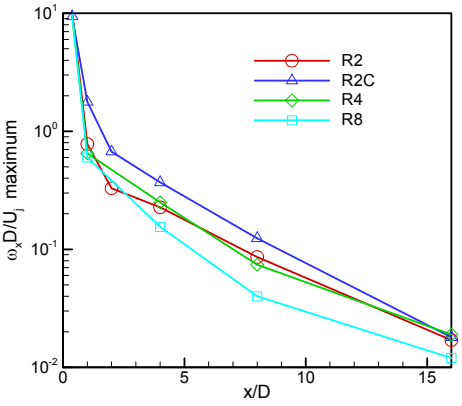

Figure 9.—Maximum (absolute) field values of streamwise vorticity as a function of axial distance.

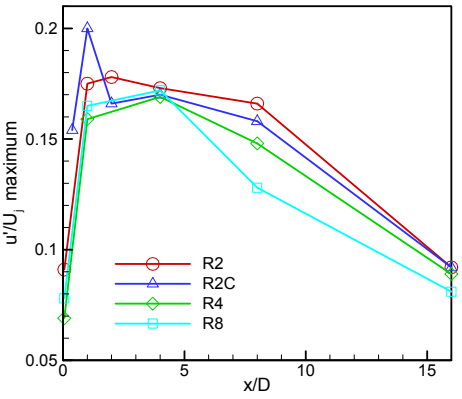

Figure 10.—Maximum field values of turbulence intensity (*u'*) as a function of axial distance.

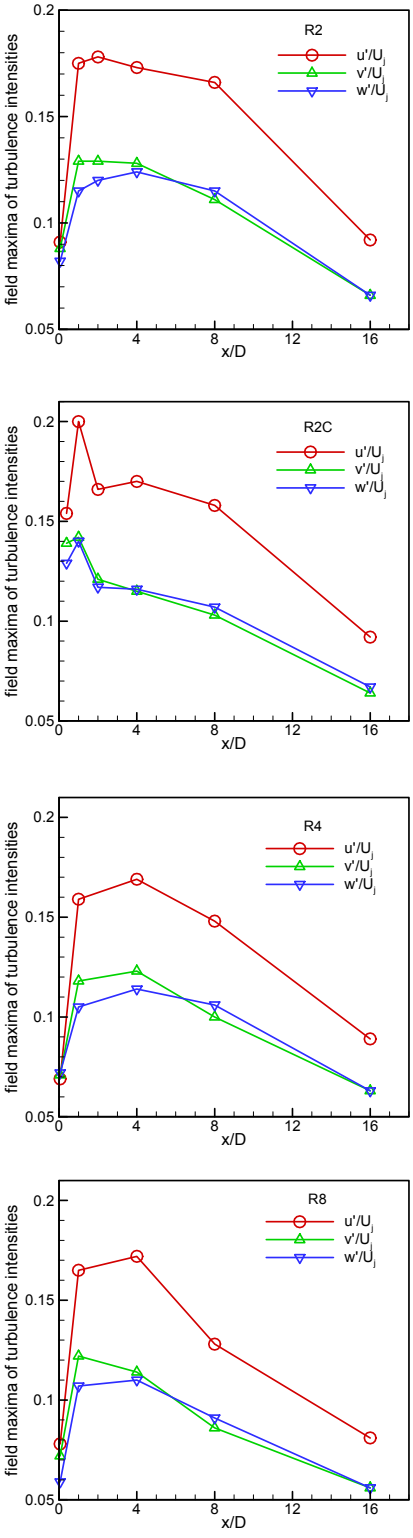

Figure 11.—Maximum field values of three components of turbulence intensity as a function of axial distance, for the nozzles as indicated.

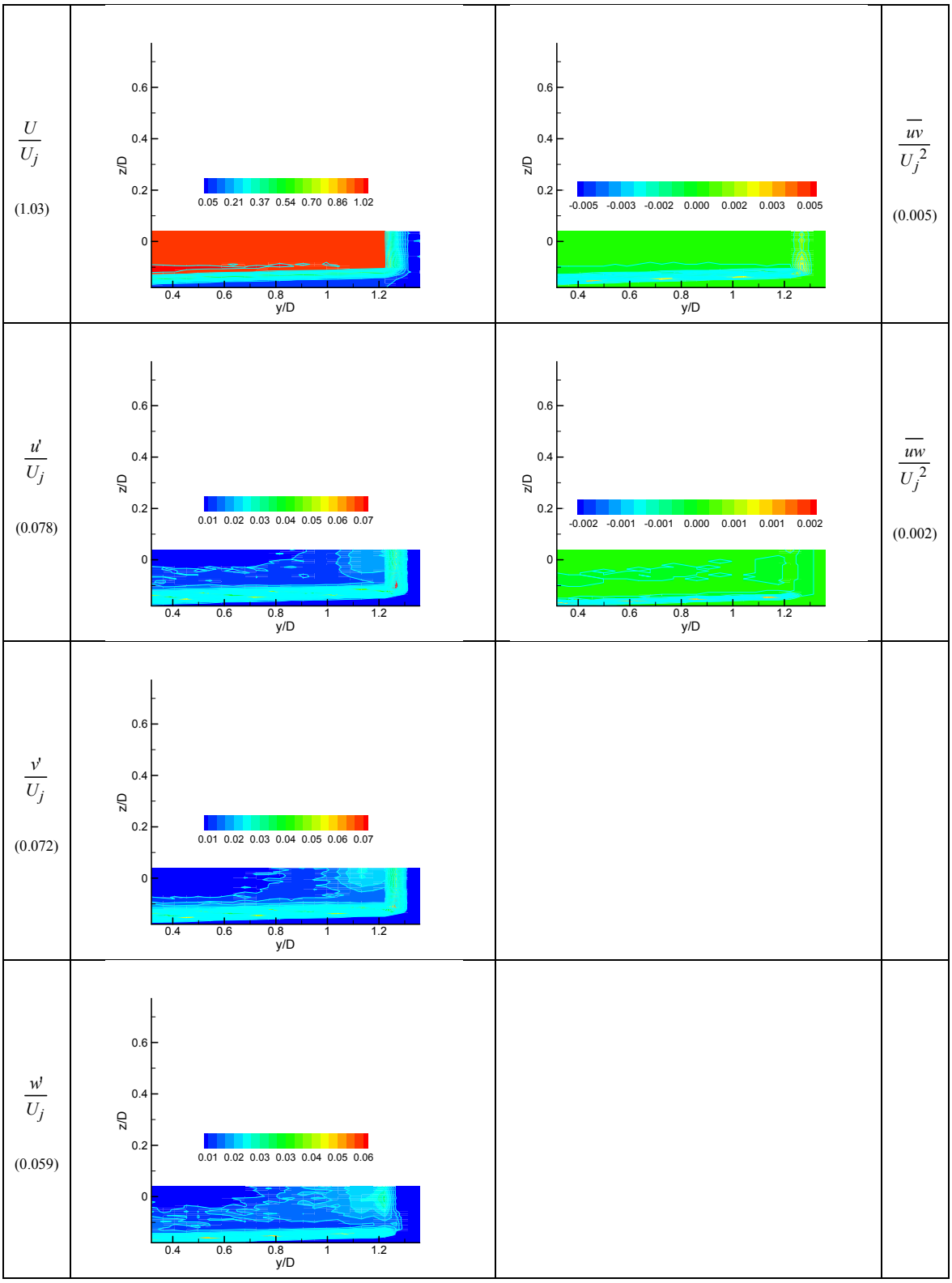

Figure A1.—For the R8 nozzle, contours of various flow properties on *y-z* plane at *x/D* = 0.05.

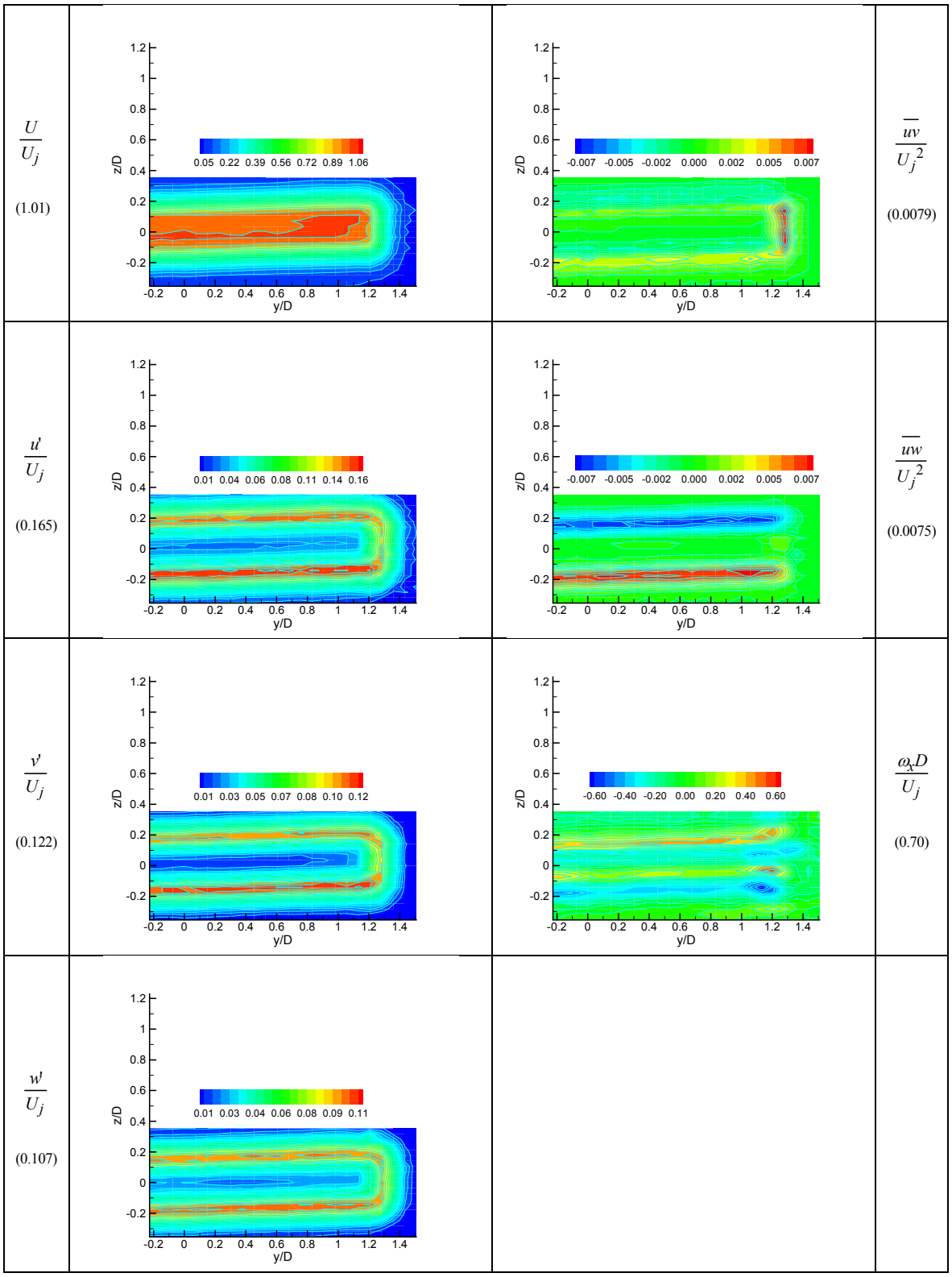

Figure A2.—For the R8 nozzle, contours of various flow properties on *y*-*z* plane at *x*/*D* = 1.

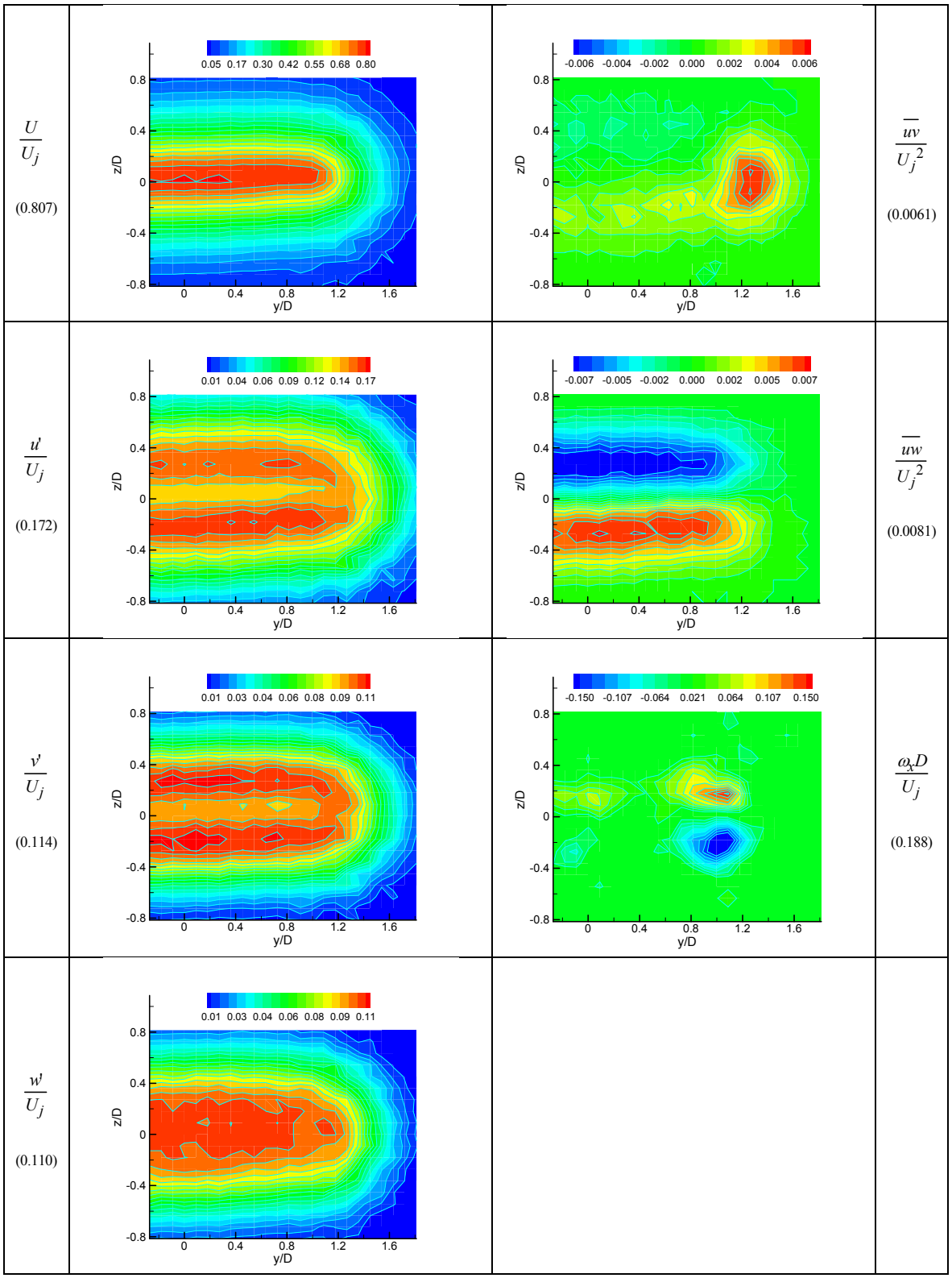

Figure A3.—For the R8 nozzle, contours of various flow properties on *y*-*z* plane at *x/D* = 4.

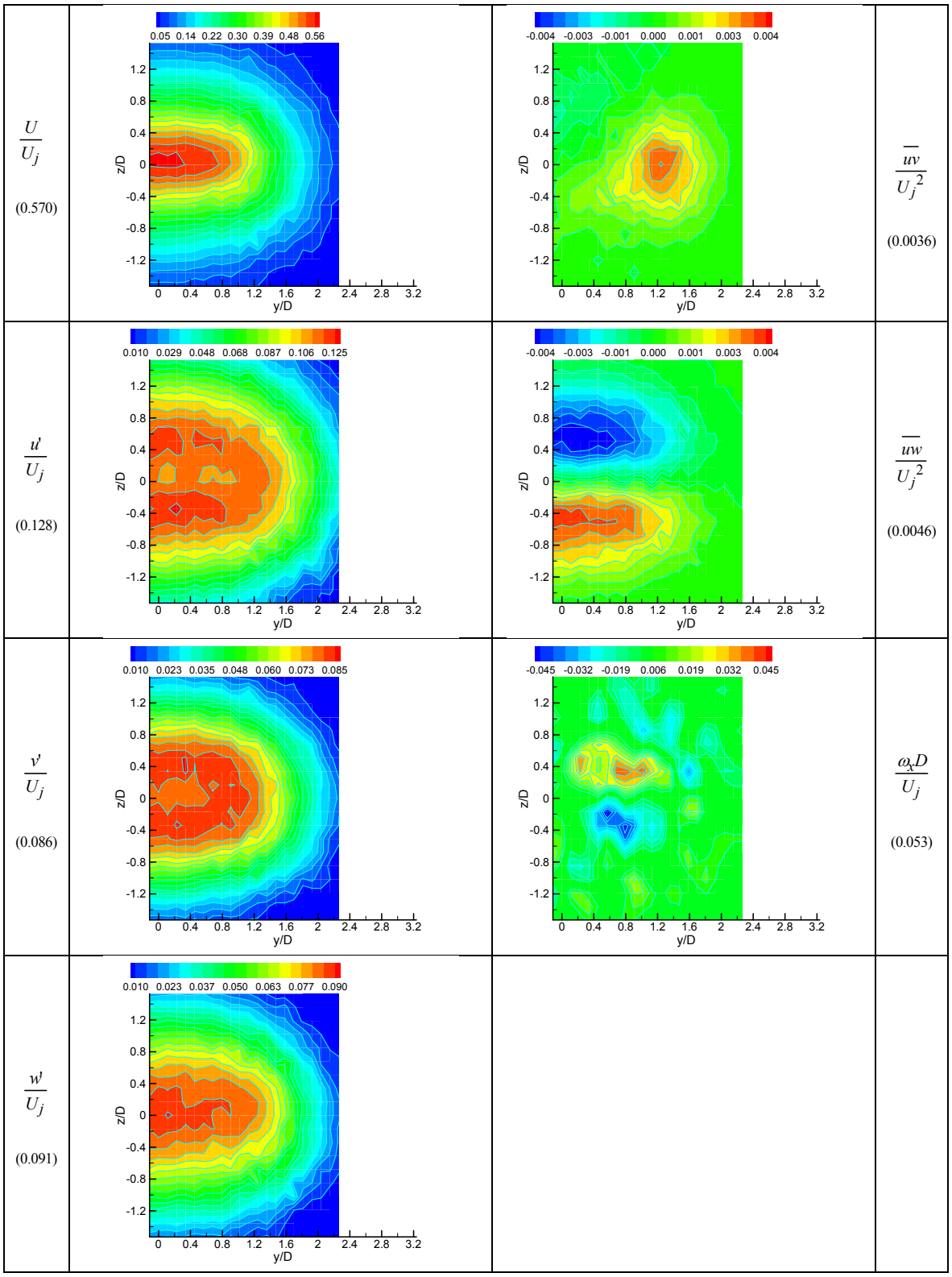

Figure A4.—For the R8 nozzle, contours of various flow properties on *y*-*z* plane at *x*/*D* = 8.

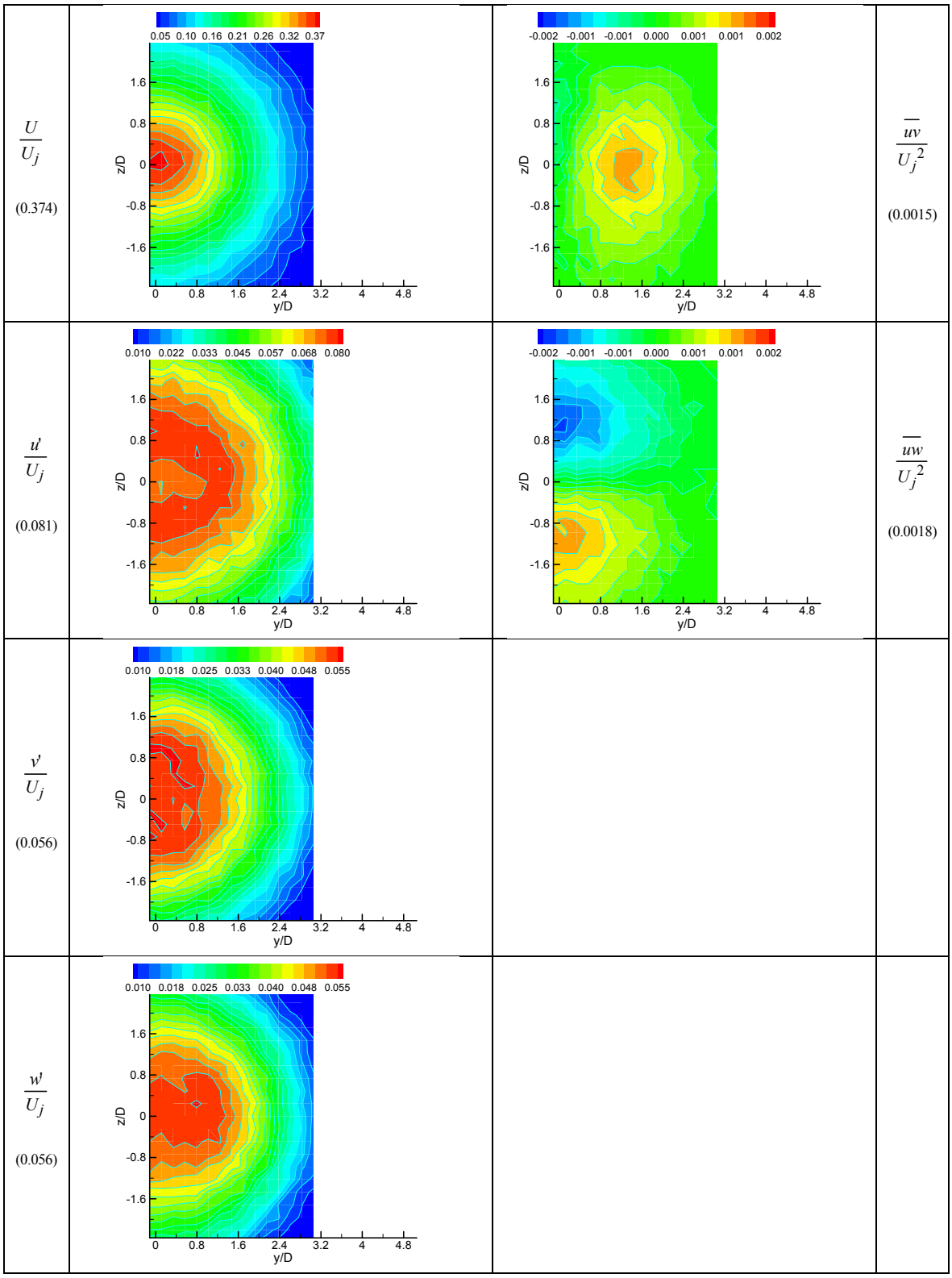

Figure A5.—For the R8 nozzle, contours of various flow properties on *y*-*z* plane at *x/D* = 16.

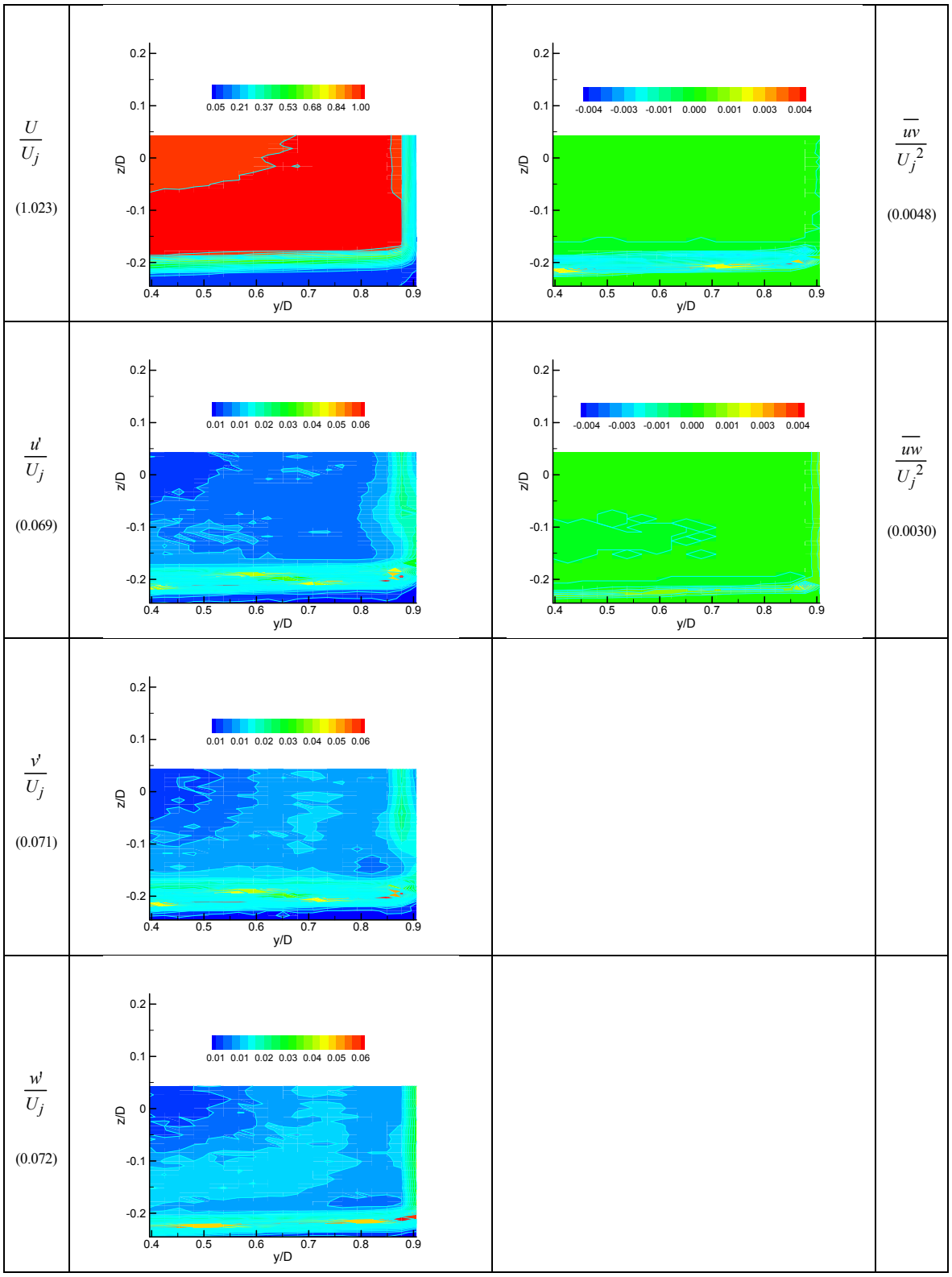

Figure A6.—For the R4 nozzle, contours of various flow properties on *y-z* plane at *x/D* = 0.05.

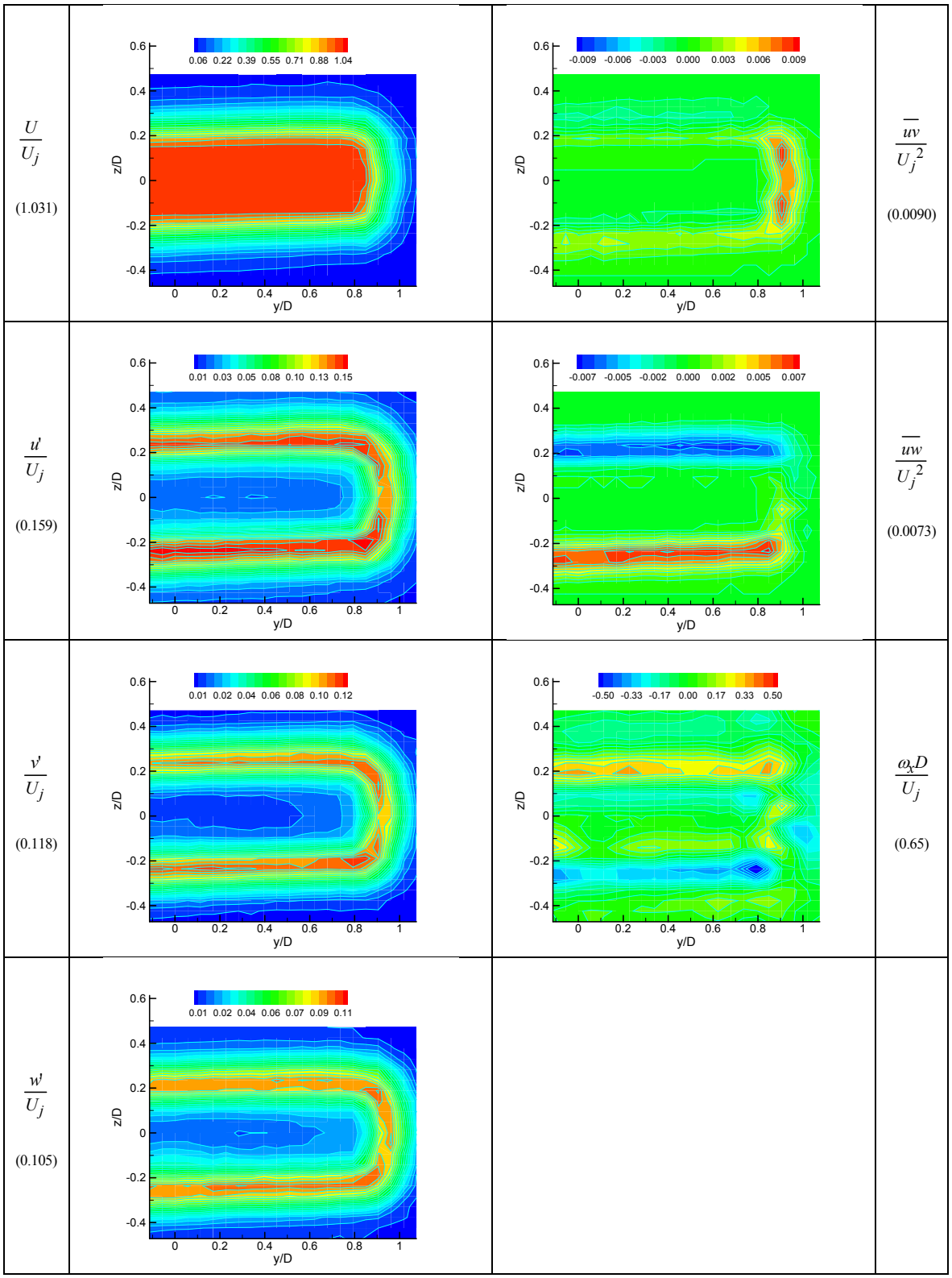

Figure A7.—For the R4 nozzle, contours of various flow properties on *y*-*z* plane at *x/D* = 1.

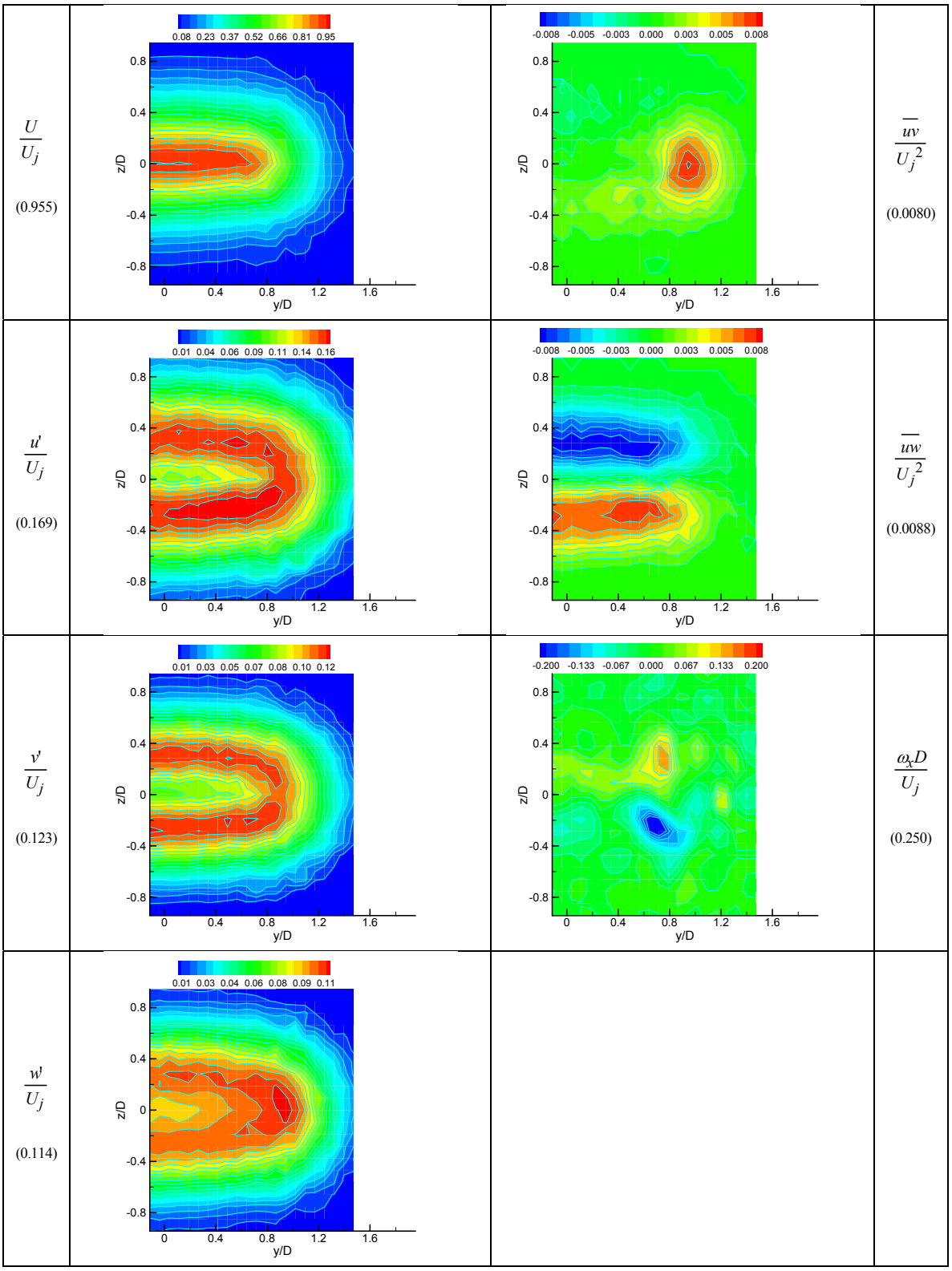

Figure A8.—For the R4 nozzle, contours of various flow properties on *y-z* plane at *x/D* = 4.

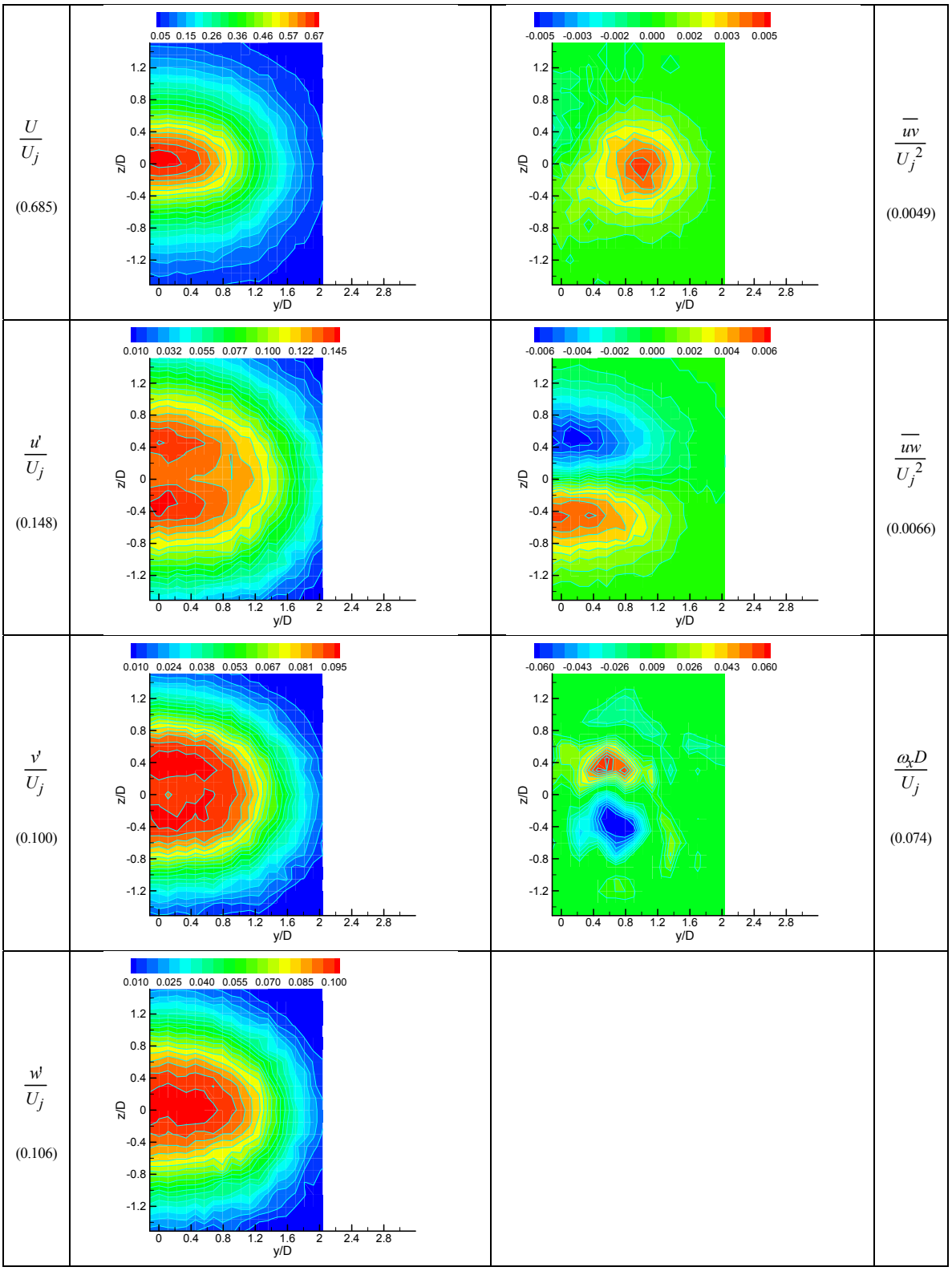

Figure A9.—For the R4 nozzle, contours of various flow properties on *y-z* plane at *x/D* = 8.

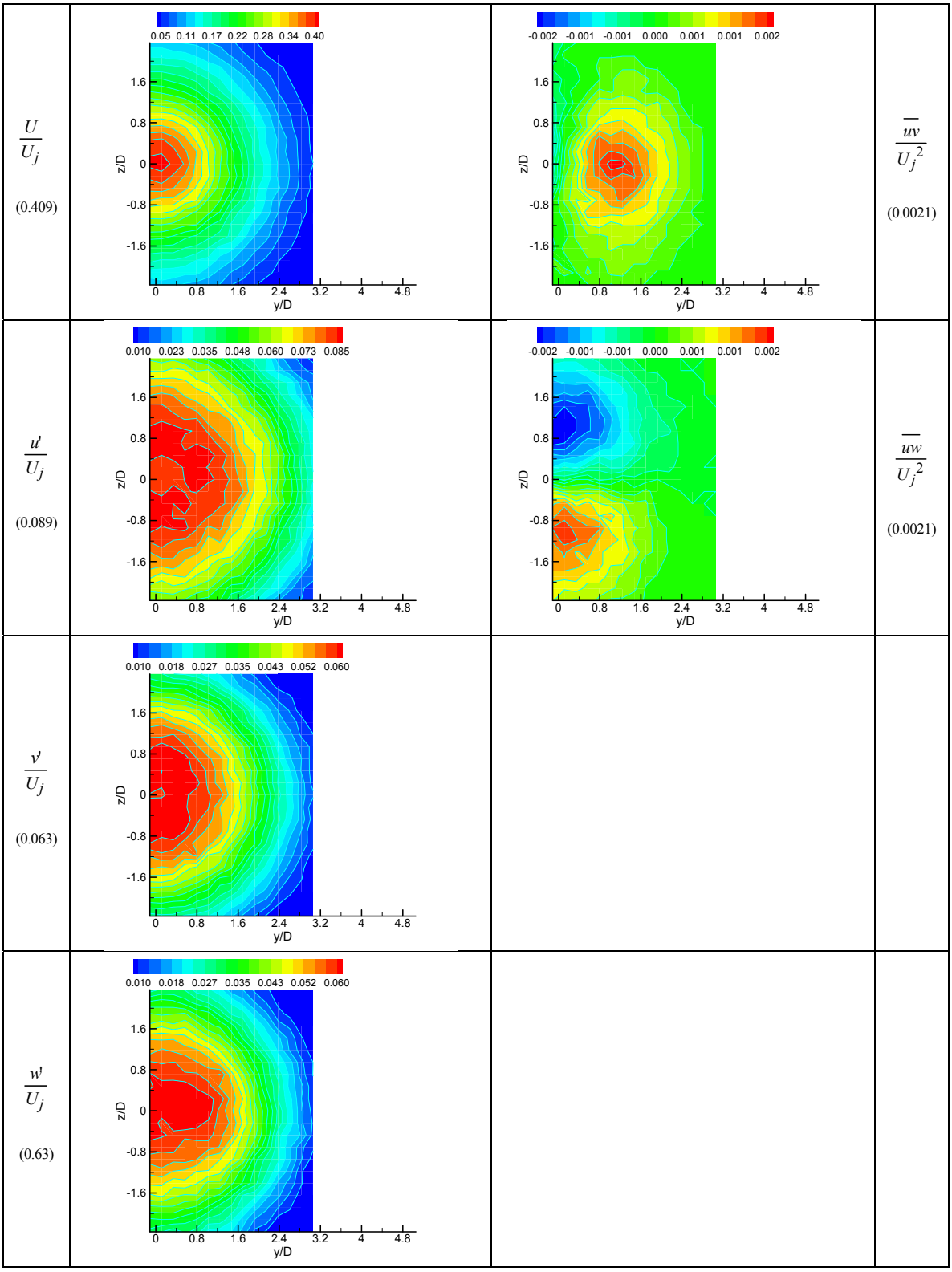

Figure A10.—For the R4 nozzle, contours of various flow properties on *y-z* plane at *x/D* = 16.

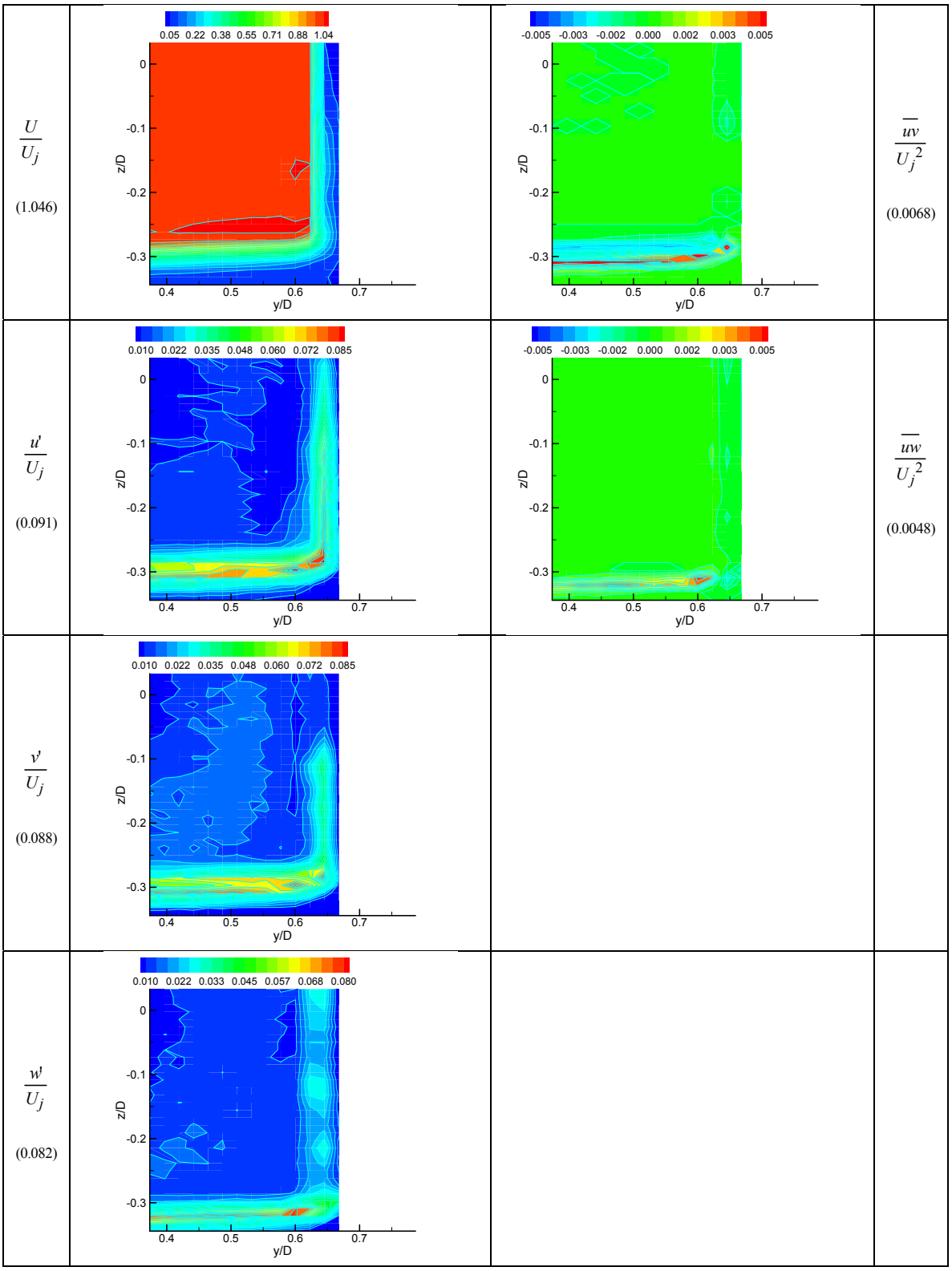

Figure A11.—For the R2 nozzle, contours of various flow properties on *y-z* plane at *x/D* = 0.05.

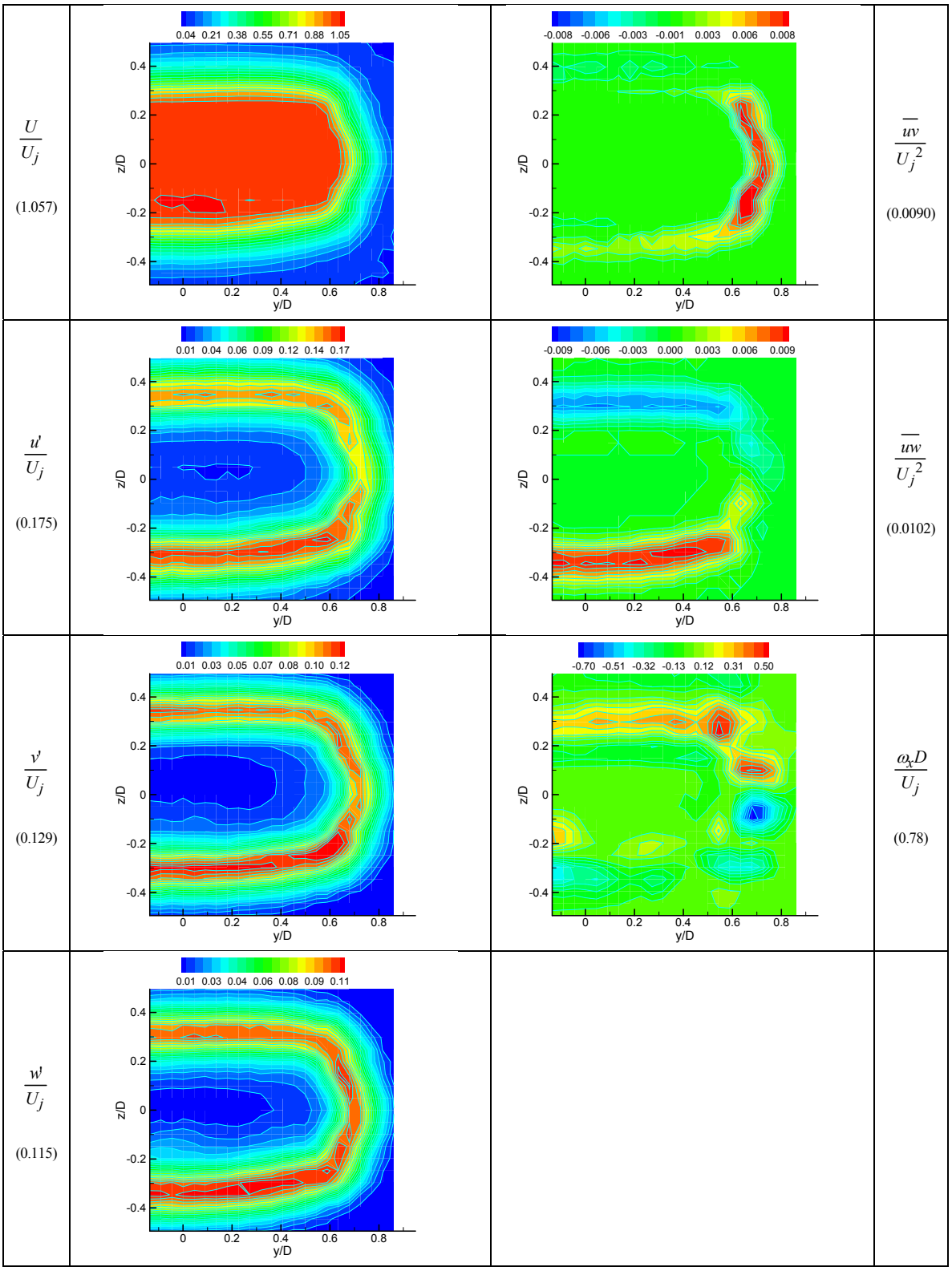

Figure A12.—For the R2 nozzle, contours of various flow properties on *y*-*z* plane at *x/D* = 1.

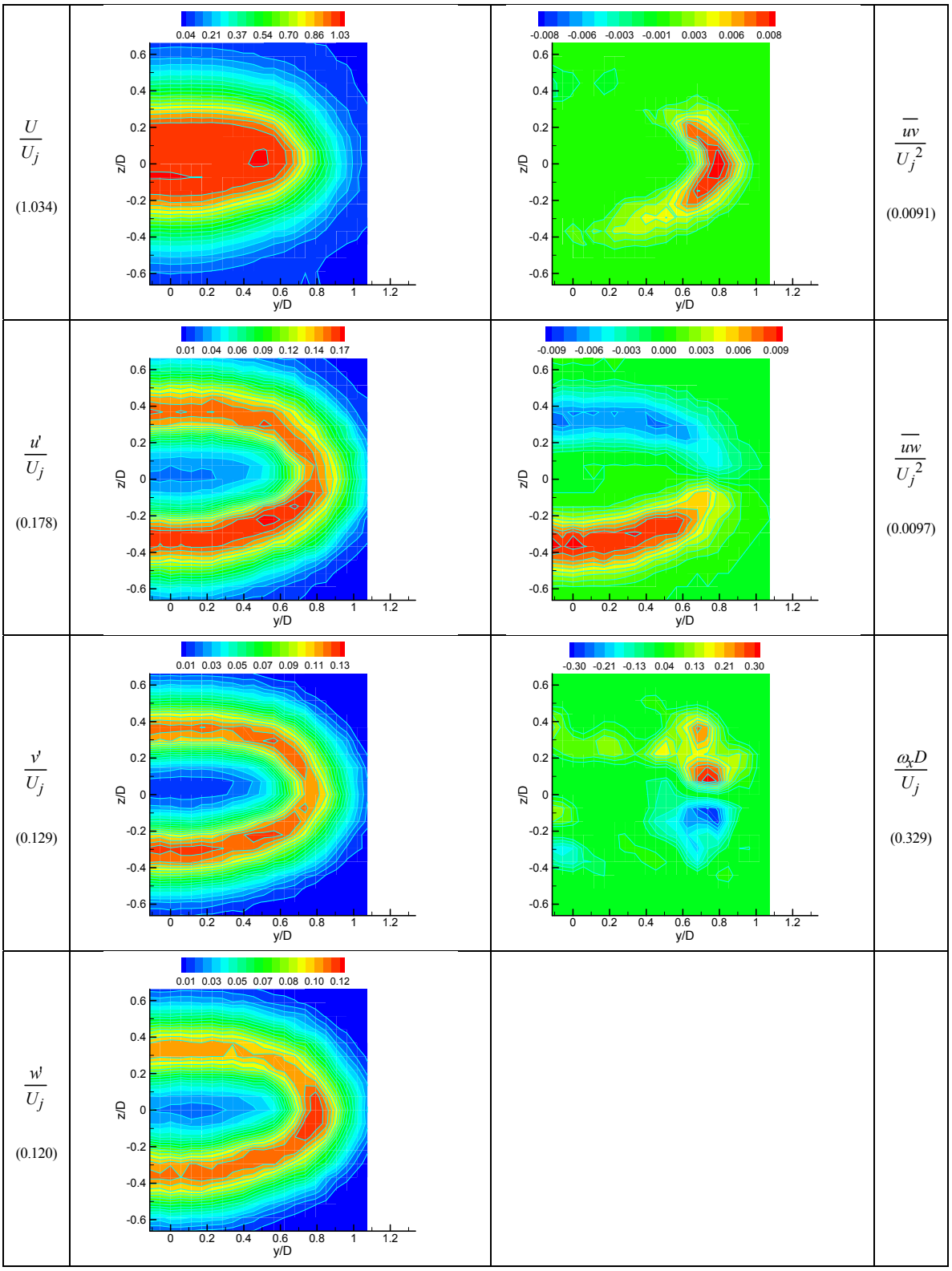

Figure A13.—For the R2 nozzle, contours of various flow properties on *y*-*z* plane at *x/D* = 2.

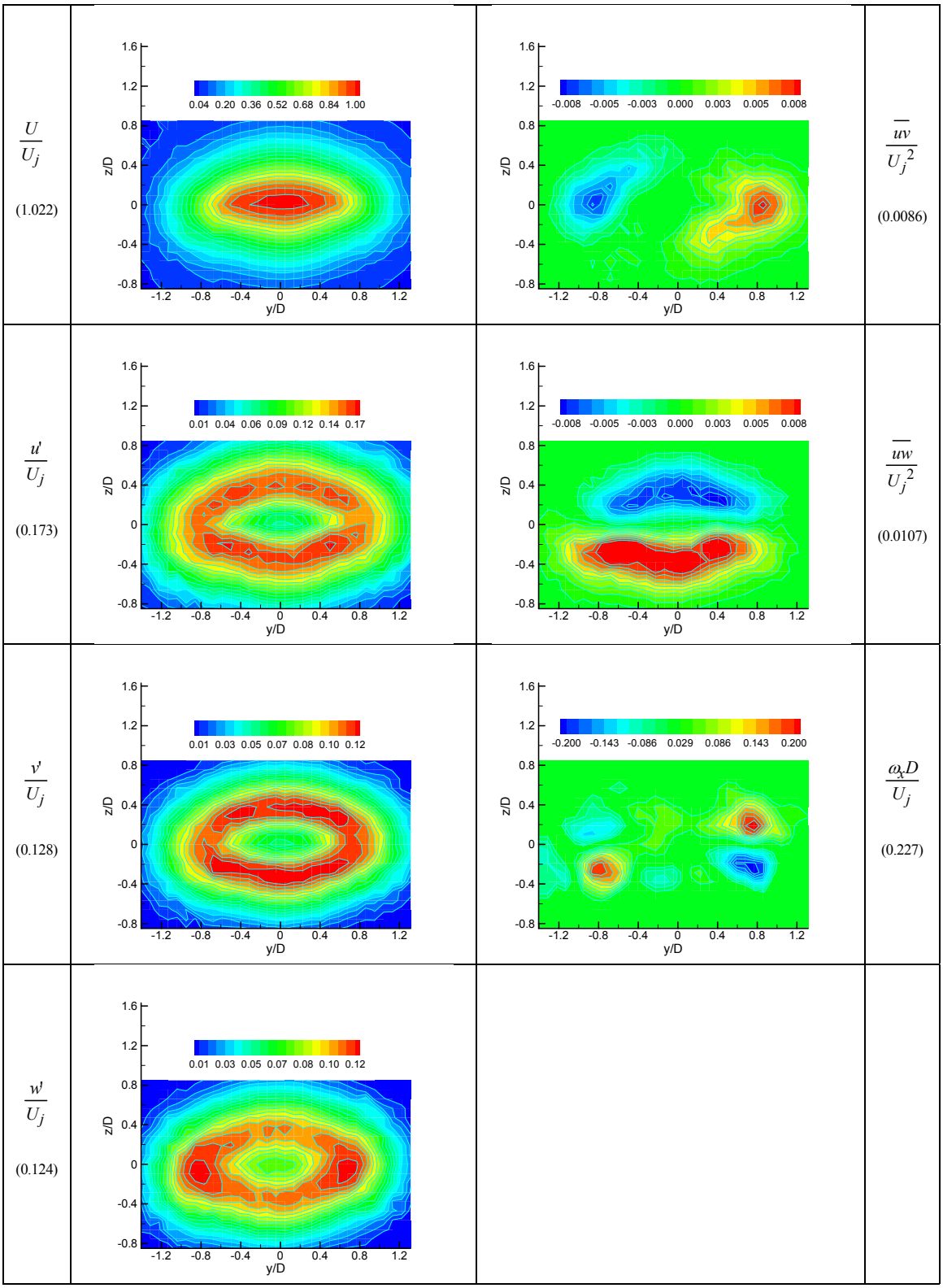

Figure A14.—For the R2 nozzle, contours of various flow properties on *y*-*z* plane at *x/D* = 4.

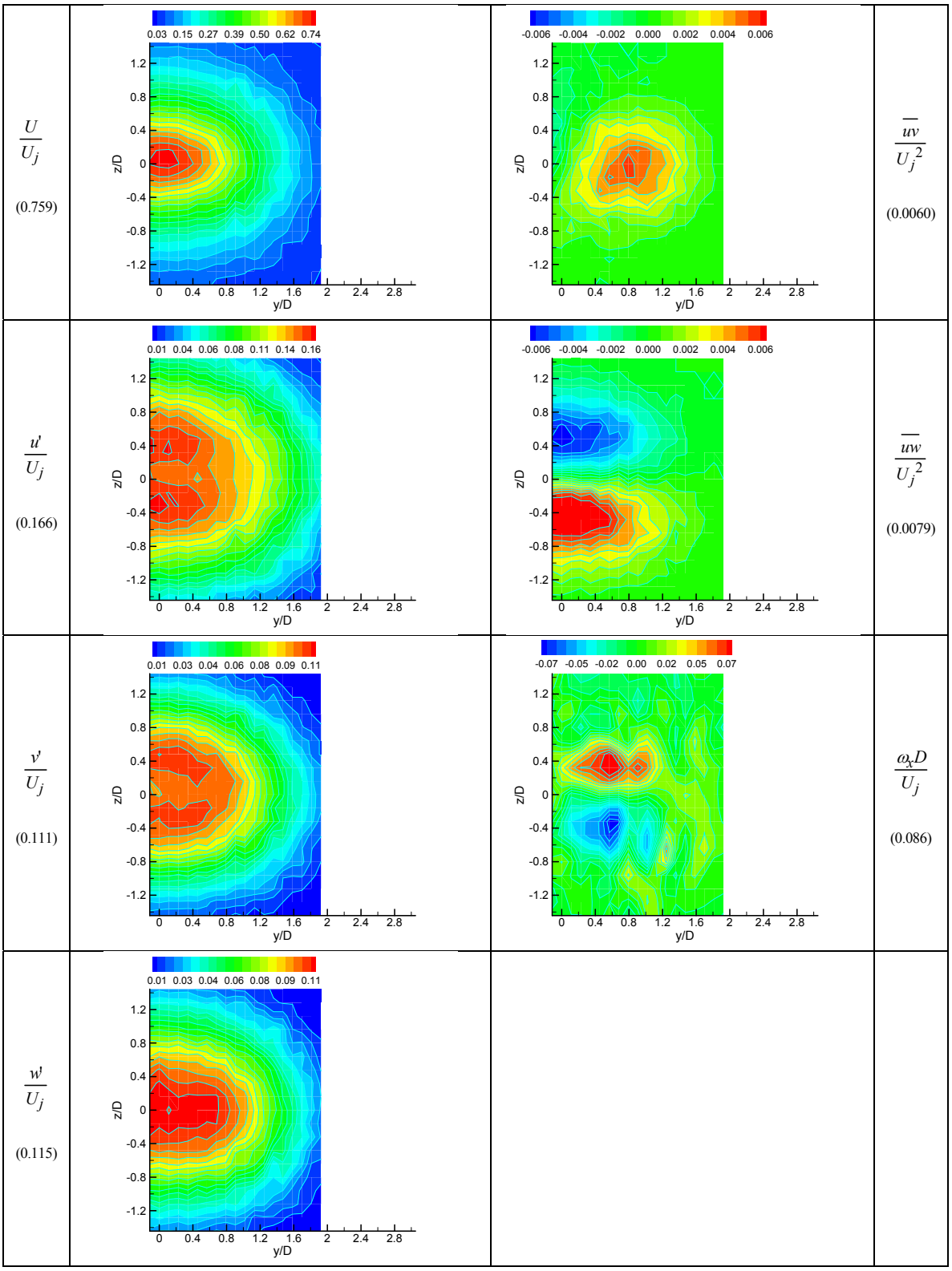

Figure A15.—For the R2 nozzle, contours of various flow properties on *y*-*z* plane at *x/D* = 8.

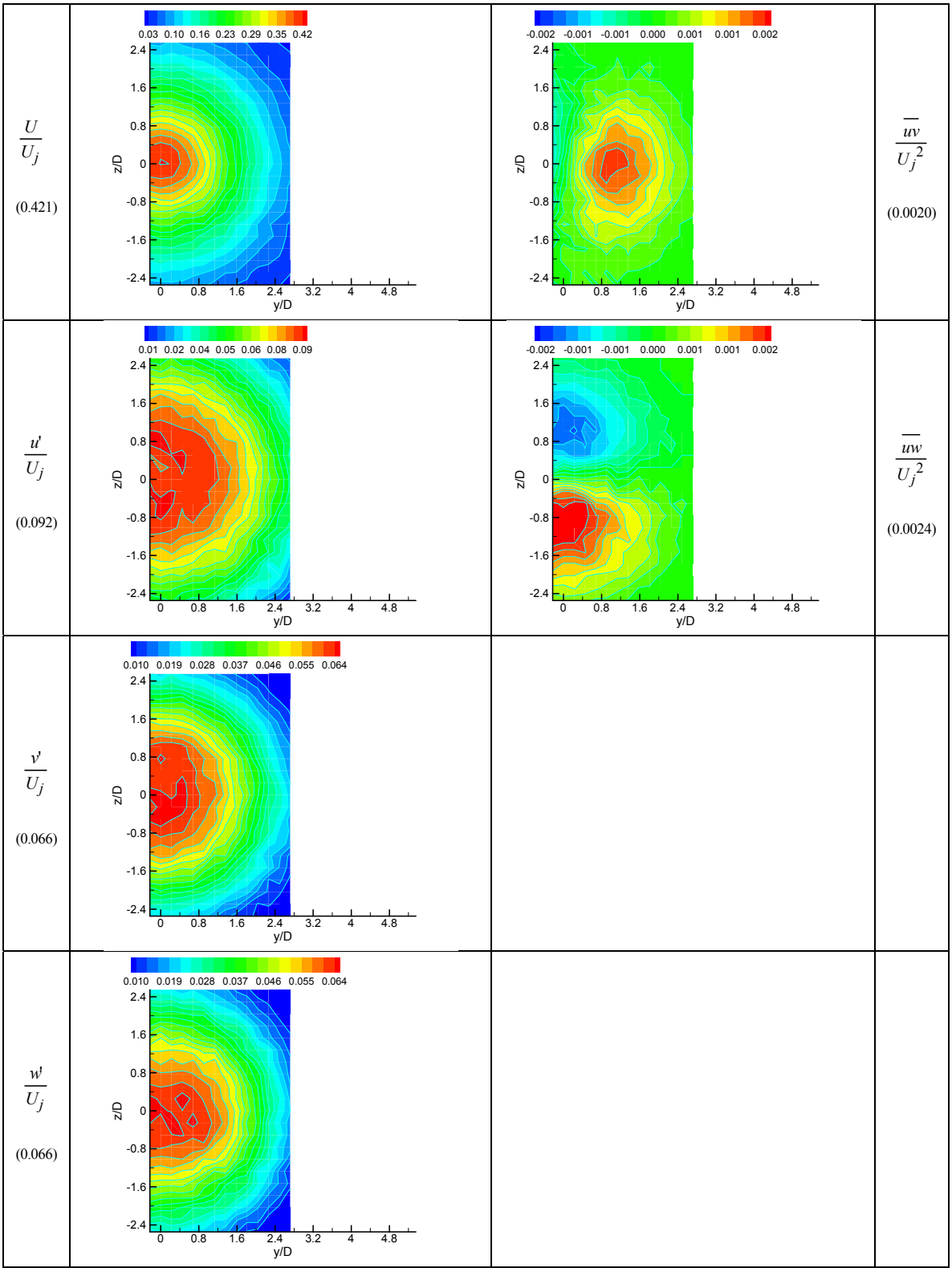

Figure A16.—For the R2 nozzle, contours of various flow properties on *y*-*z* plane at *x/D* = 16.

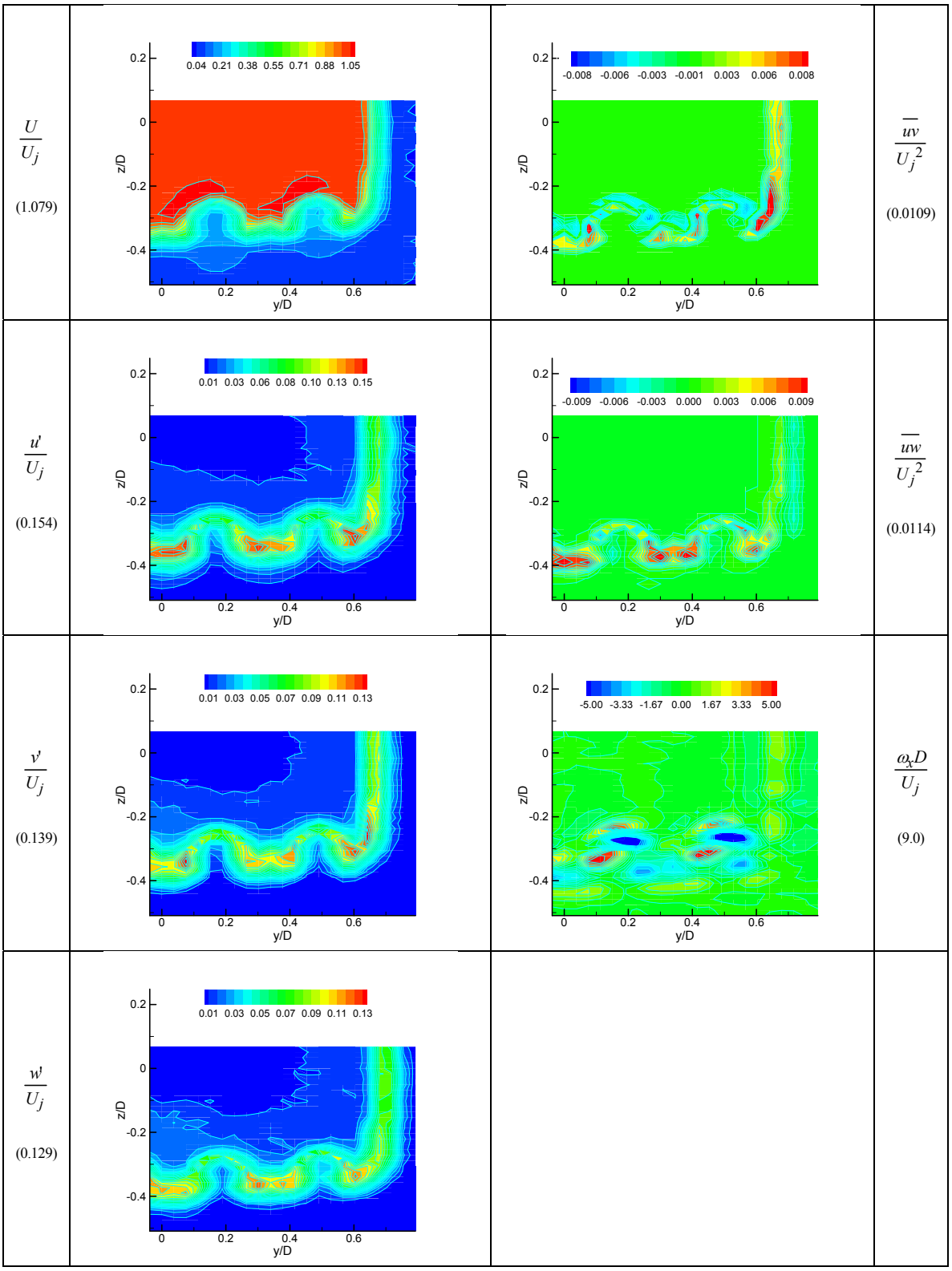

Figure A17.—For the R2C nozzle, contours of various flow properties on *y-z* plane at *x/D* = 0.38.

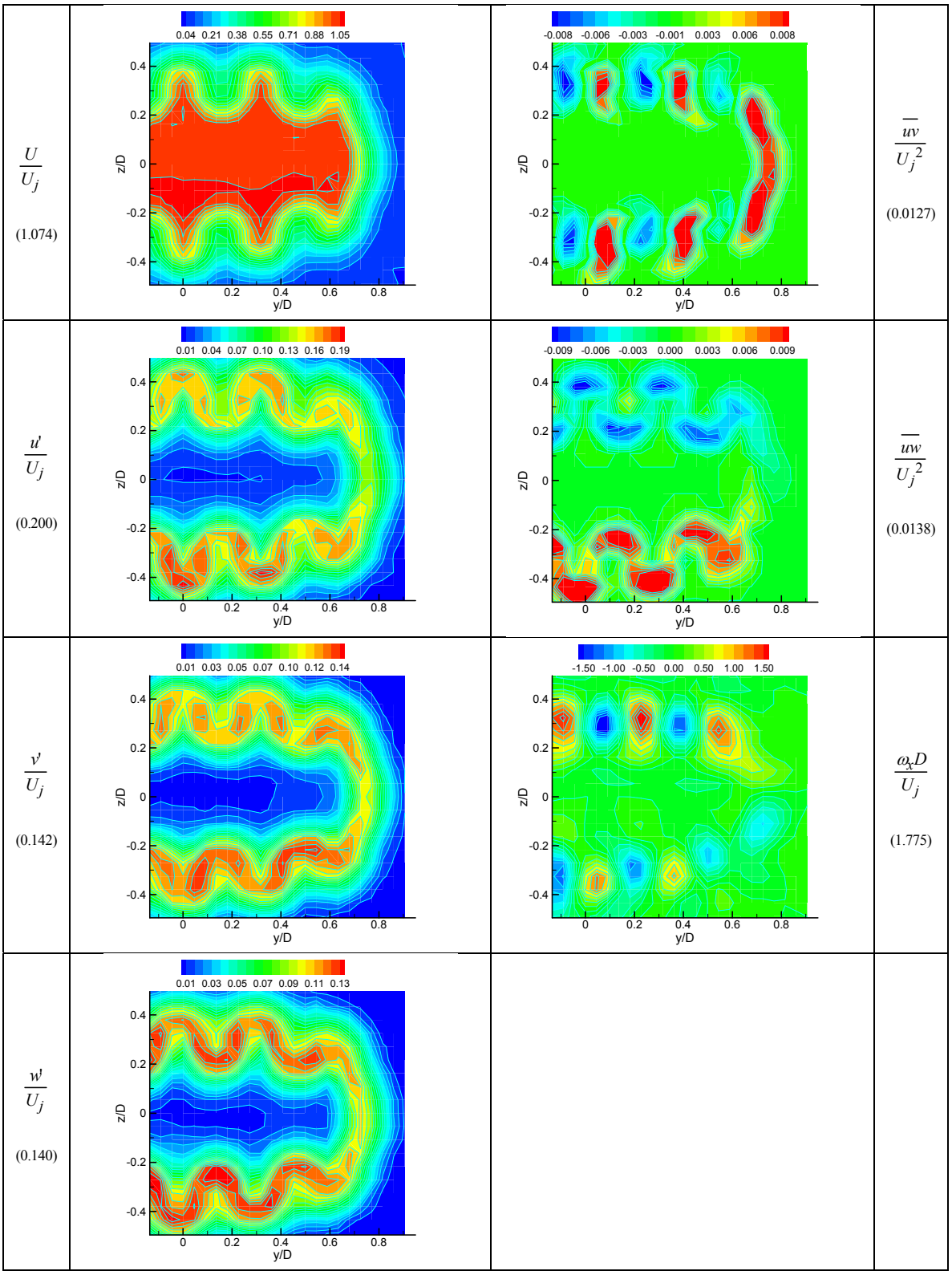

Figure A18.—For the R2C nozzle, contours of various flow properties on *y-z* plane at *x/D* = 1.

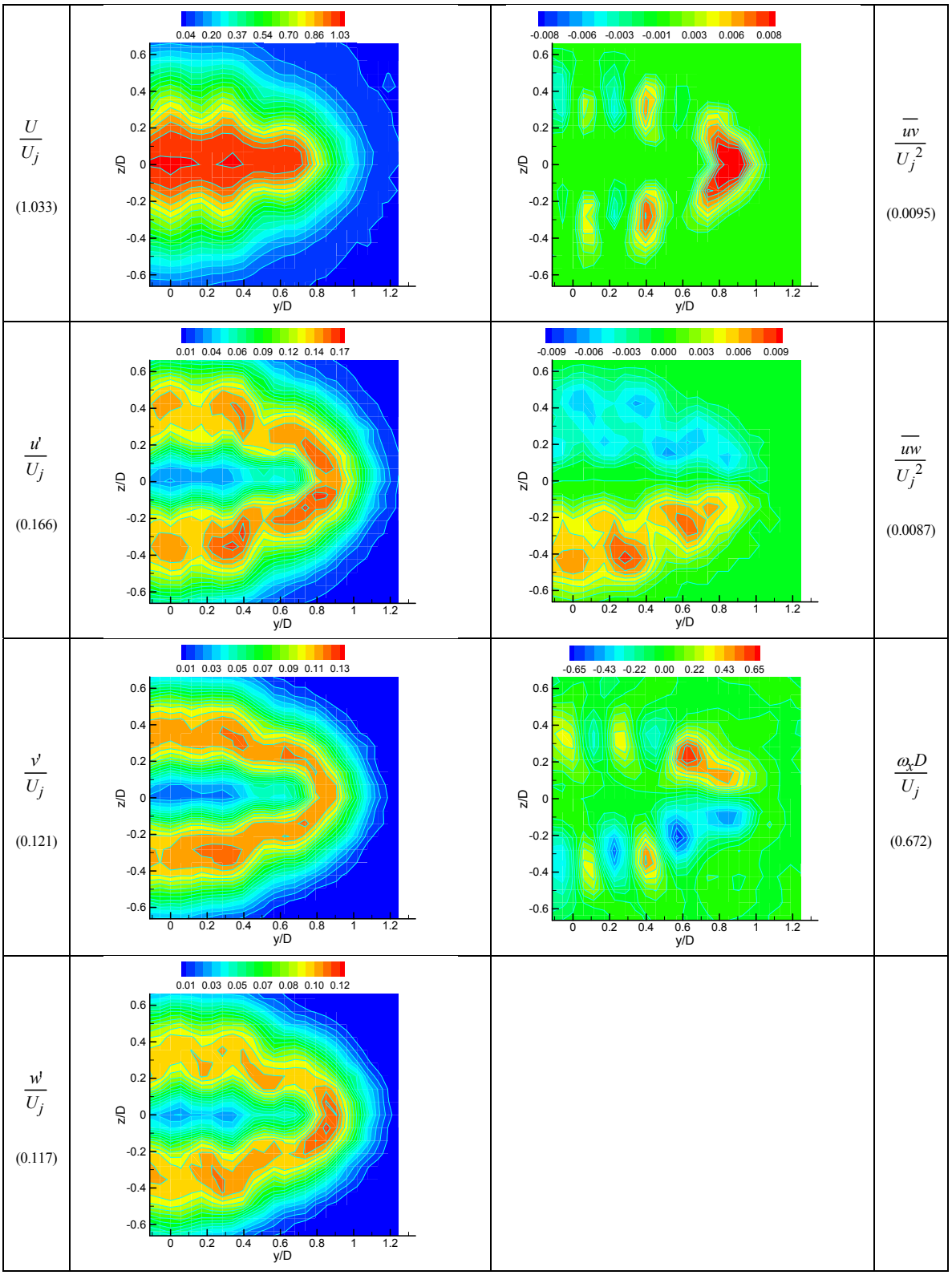

Figure A19.—For the R2C nozzle, contours of various flow properties on *y-z* plane at *x/D* = 2.

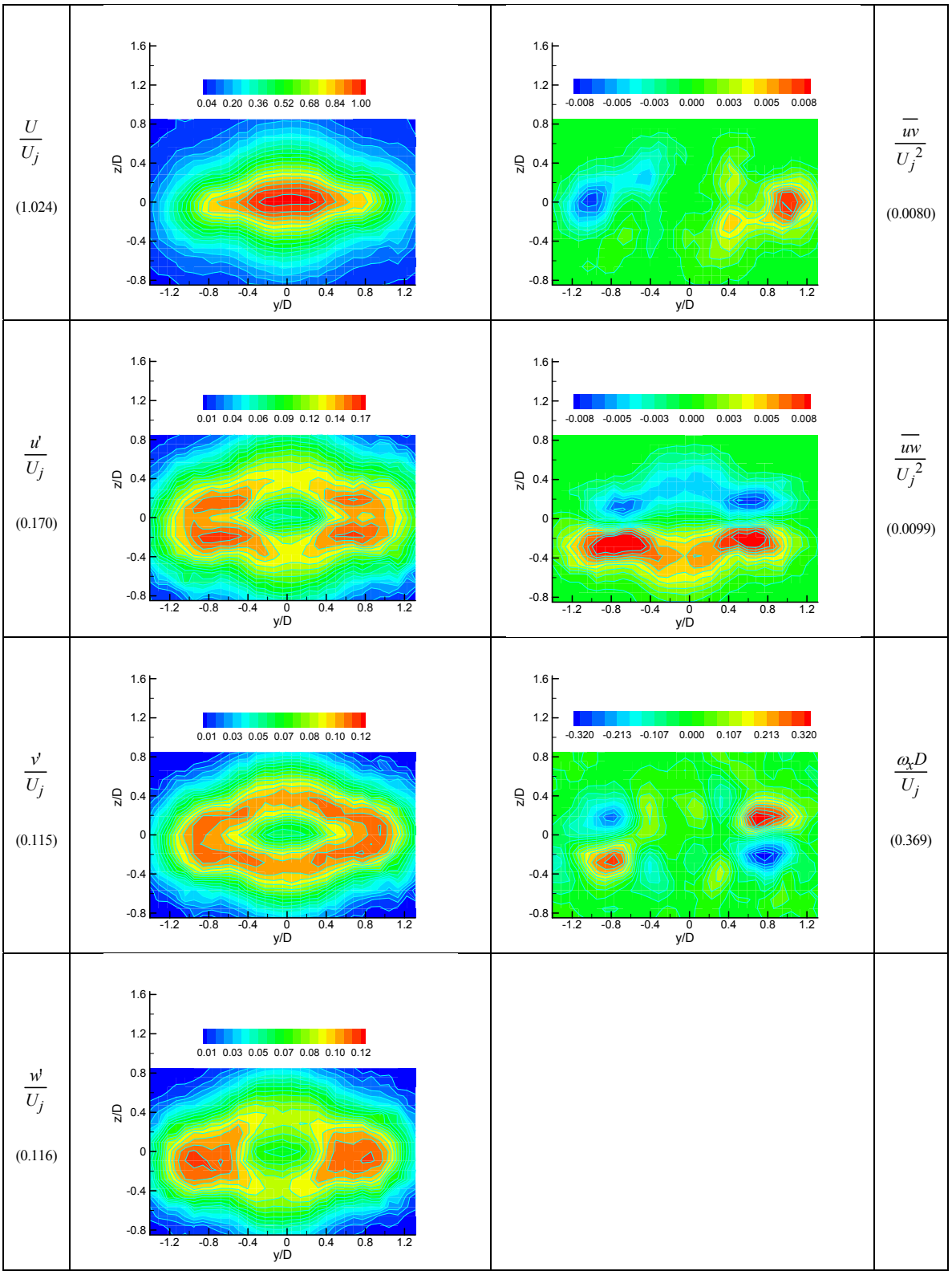

Figure A20.—For the R2C nozzle, contours of various flow properties on *y-z* plane at *x/D* = 4.

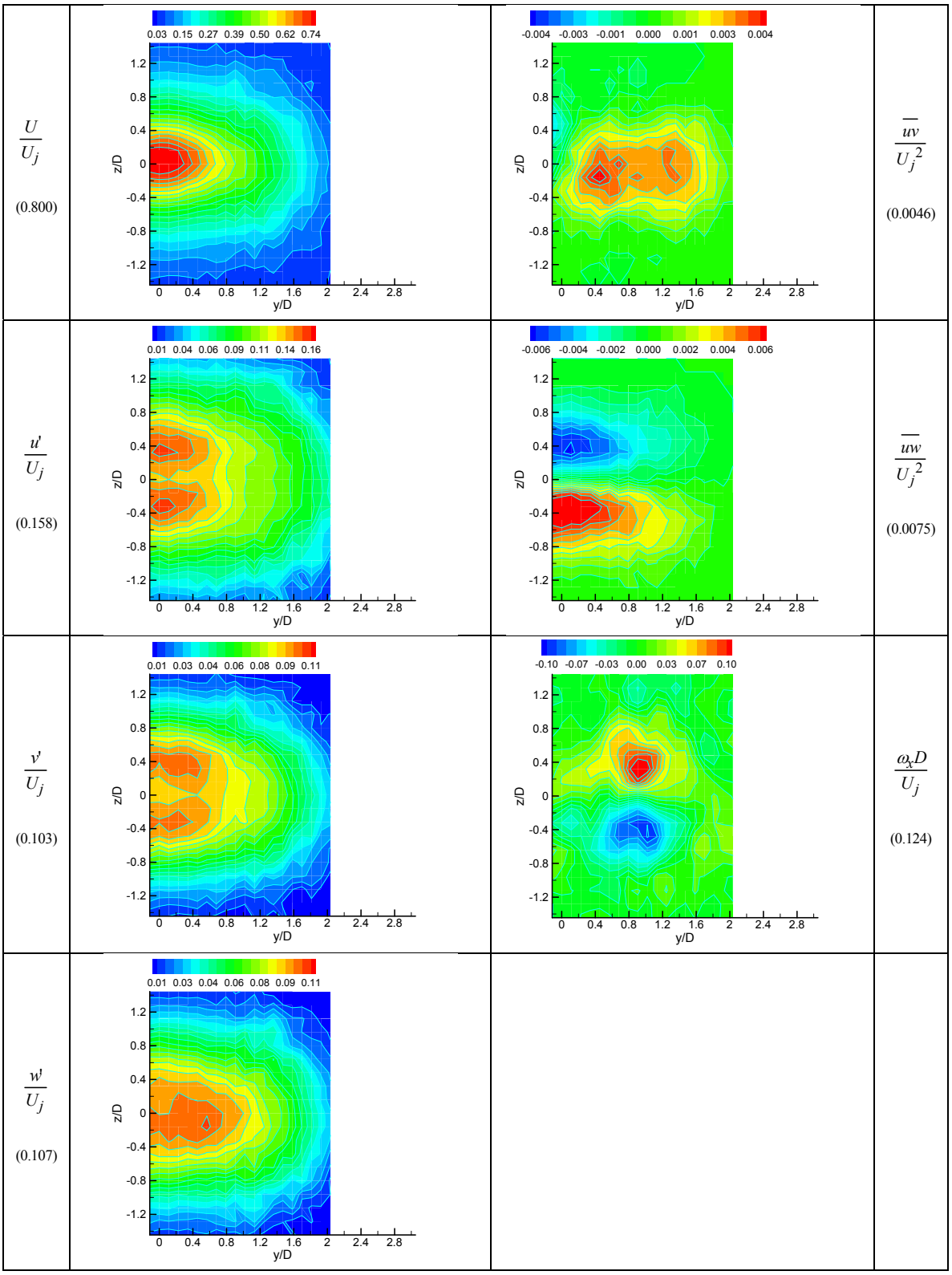

Figure A21.—For the R2C nozzle, contours of various flow properties on *y-z* plane at *x/D* = 8.

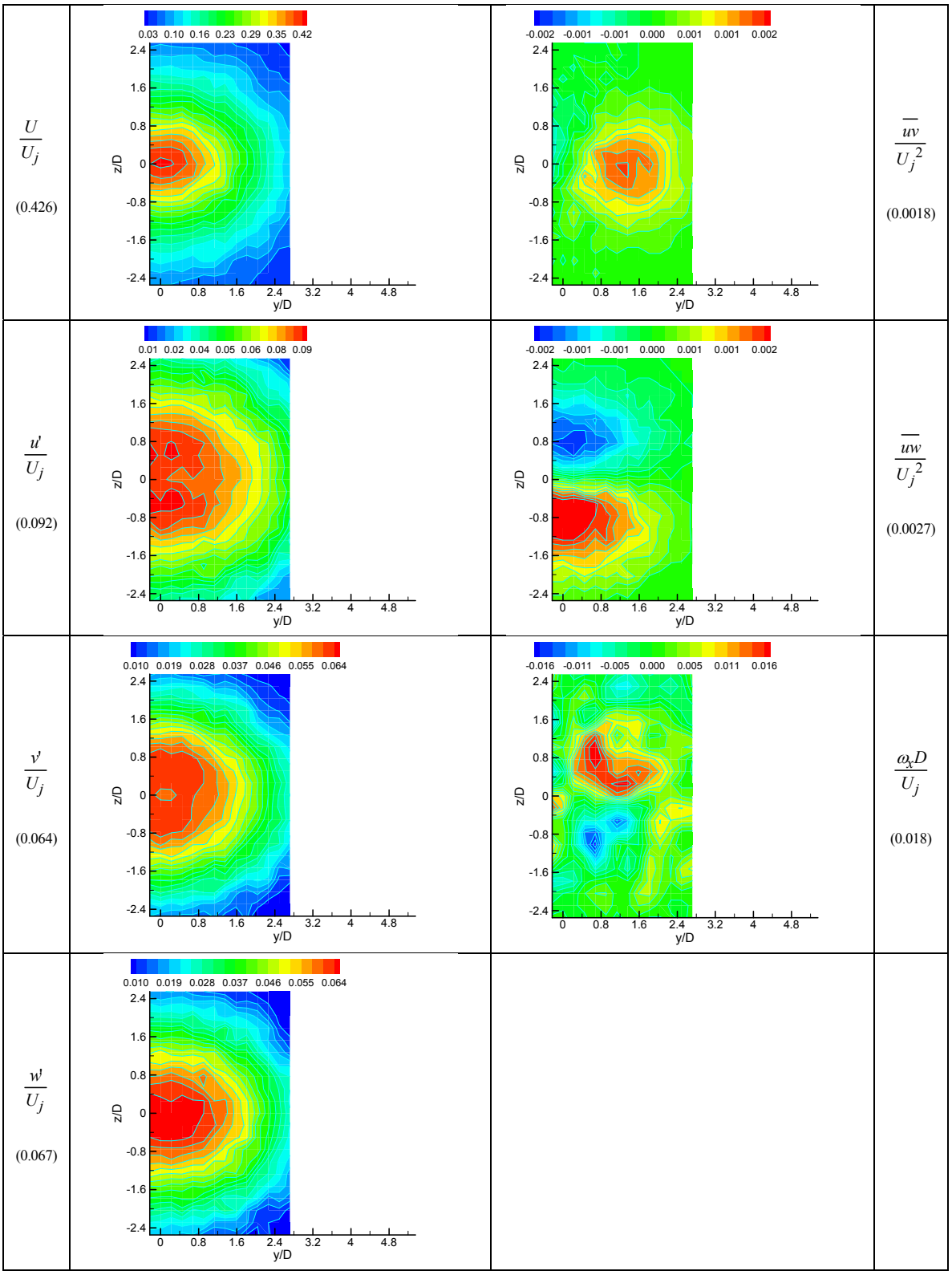

Figure A22.—For the R2C nozzle, contours of various flow properties on *y-z* plane at *x/D* = 16.

References

1. Bridges, J.E., "Noise of embedded high-aspect ratio nozzles," presented at the NASA Fundamental Aeronautics Program 2011 Technical Conference, Cleveland, OH, March 15-17, 2011.
2. Balsa, T.F., Gliebe, R.R., Kantola, R.A., Mani, R., Stringas, E.J. and Wang, J.C.F., "High velocity jet noise source location and reduction, Task 2—theoretical developments and basic experiments," Report No. FAA-RD-76-79, II, General Electric Co., Aircraft Engine Group, Cincinnati, OH, May, 1978.
3. Massey, K.C., Ahuja, K.K. and Gaeta, R., "Noise Scaling for Unheated Low Aspect Ratio Rectangular Jets," AIAA paper 2004-2946, 10th AIAA/CEAS Aeroacoustics Conference, Manchester, England 10-12 May 2004.
4. Frate, F.C. and Bridges, J.E., "Extensible rectangular nozzle model system," AIAA Paper 2011-975, 49th Aerospace Sciences Meeting, Orlando, Fl, 4-7 January, 2011.
5. Zaman, K.B.M.Q., 2012, "Flow field surveys for rectangular nozzles," AIAA Paper 2012-0069, 50th AIAA Aerospace Sciences Meeting, January 9-12, Nashville, TN.
6. Zaman, K.B.M.Q., 1996, "Axis switching and spreading of an asymmetric jet: the role of coherent structure dynamics." 1966, *J. Fluid Mech., 316*, pp. 1-27.
7. Zaman, K.B.M.Q., 2011, "Effect of nozzle exit conditions on subsonic jet noise," AIAA Paper 2011-2704, 17th AIAA/CEAS Aeroacoustics Conf., 5-8 June, Portland, Oregon.
8. Morris, P.J. & Zaman, K.B.M.Q., "Velocity measurements in jets with application to noise source modeling," *Journal of Sound and Vibration* (2009),doi:10.1016/j.jsv.2009.09.024.
9. Zaman, K.B.M.Q., 1998, "Asymptotic spreading rate of initially compressible jets—experiment and analysis," *Physics of Fluids*, *10*, pp. 2652-2660.

REPORT DOCUMENTATION PAGE			Form Approved OMB No. 0704-0188

1. REPORT DATE *(DD-MM-YYYY)*	2. REPORT TYPE	3. DATES COVERED *(From - To)*
01-04-2012	Technical Memorandum	

4. TITLE AND SUBTITLE
Flow-Field Surveys For Rectangular Nozzles

5a. CONTRACT NUMBER

5b. GRANT NUMBER

5c. PROGRAM ELEMENT NUMBER

6. AUTHOR(S)
Zaman, K.B.M.Q.

5d. PROJECT NUMBER

5e. TASK NUMBER

5f. WORK UNIT NUMBER
WBS 984754.02.07.03.17.04

7. PERFORMING ORGANIZATION NAME(S) AND ADDRESS(ES)
National Aeronautics and Space Administration
John H. Glenn Research Center at Lewis Field
Cleveland, Ohio 44135-3191

8. PERFORMING ORGANIZATION REPORT NUMBER
E-18082

9. SPONSORING/MONITORING AGENCY NAME(S) AND ADDRESS(ES)
National Aeronautics and Space Administration
Washington, DC 20546-0001

10. SPONSORING/MONITOR'S ACRONYM(S)
NASA

11. SPONSORING/MONITORING REPORT NUMBER
NASA/TM-2012-217410

12. DISTRIBUTION/AVAILABILITY STATEMENT
Unclassified-Unlimited
Subject Categories: 71 and 34
Available electronically at http://www.sti.nasa.gov
This publication is available from the NASA Center for AeroSpace Information, 443-757-5802

13. SUPPLEMENTARY NOTES
A CD-ROM containing the supplemental data files mentioned in the Introduction section of this report can be requested from the NASA Center for AeroSpace Information at http://www.sti.nasa.gov, or 443-757-5802.

14. ABSTRACT
Flow field survey results for three rectangular nozzles are presented for a low subsonic condition obtained primarily by hot-wire anemometry. The three nozzles have aspect ratios of 2:1, 4:1 and 8:1. A fourth case included has 2:1 aspect ratio with chevrons added to the long edges. Data on mean velocity, turbulent normal and shear stresses as well as streamwise vorticity are presented covering a streamwise distance up to sixteen equivalent diameters from the nozzle exit. These detailed flow properties, including initial boundary layer characteristics, are usually difficult to measure in high speed flows and the primary objective of the study is to aid ongoing and future computational and noise modeling efforts.

15. SUBJECT TERMS
Aeroacoustics; Jet noise; Turbulence

16. SECURITY CLASSIFICATION OF:			17. LIMITATION OF ABSTRACT	18. NUMBER OF PAGES	19a. NAME OF RESPONSIBLE PERSON
a. REPORT	b. ABSTRACT	c. THIS PAGE			STI Help Desk (email:help@sti.nasa.gov)
U	U	U	UU	39	19b. TELEPHONE NUMBER *(include area code)* 443-757-5802